rat CD1d are designated as P80rCD80rCD1d, those transduced with mouse CD1d as P80rCD80mCD1d.

Mouse CD1d was cloned from A20mCD1d cell line (38) by RT-PCR using the following primers: mCD1d-*Eco*RI-Fow (5'-GGG GAG AAT TCC GGC GCT ATG CGG TAC CTA CC-3'); and mCD1d-*Eco*RI-Rev (5'-GGT GGA ATT CAG AGT CAC CGG ATG TCT TGA TAA G-3'). The sequence of the insert showed a complete overlap with the mouse CD1d sequence available in the gene bank under X13170 (39). Rat CD1d cDNA was obtained by RT-PCR using RNA isolated from F344/Crl rat bone marrow as a template and CD1d-specific primers: N366 (5'-TCG GAG CCC AGG GCT GTG TAG A-3'); and rCD1dRev (5'-TTC TGA GCA GAC AAG GAC TGA-3'). PCR product was cloned into TOPO cloning vector and sequenced. The sequence was identical with rat CD1d (GenBank accession number AB029486) published by Katabami et al. (23). Mouse and rat CD1d DNA were cloned into *Eco*RI site of pczCGZ51Z and pczCGZ5 IEGZ vectors, respectively, and were further used for retroviral infection of P80rCD80 cells.

The expression of mouse CD1d was tested with the CD1d-specific mAb 1B1 (BD Pharmingen), whereas expression of rat CD1d was assessed from the green fluorescence of the *EGFP* reporter gene. Surface expression of rat CD1d was also confirmed with a novel rat CD1d-specific mAb (E. Pyz and T. Herrmann, unpublished observations). The Ag-presenting cell lines were enriched for CD1d expression by cell sorting or selection with antibiotics.

Stimulation with α-GalCer in vitro

α-GalCer was generated as described (40). The reactivity of mouse and rat IHLs to α-GalCer was tested by culture of IHL (1×10^5 cells/well of a 96-well round-bottom plate) in the presence of α-GalCer (100 ng/ml), vehicle (DMSO), or complete medium for 24 h at 37°C. The level of IL-4 and IFN-γ released into culture supernatants was determined using ELISA kits (BD Pharmingen).

To analyze the α-GalCer reactivity of TCR-transduced cell lines, mouse and rat thymocytes (1×10^6 cells/well), or CD1d-transduced cells (P80mCD1drCD80, P80rCD1drCD80, 5×10^4 cell/well) used as APC were loaded with either α-GalCer (1–100 ng/ml) or vehicle (DMSO) for 1–2 h before the addition of responder cells. As a positive control, TCR-positive cell lines were stimulated with plate-bound anti-mouse CD3 mAb 145C11. After 24 h of culture, supernatants were taken, and the secreted mouse IL-2 was quantified using a commercial ELISA Kit (BD Pharmingen).

Immunofluorescence and flow cytometry

For the staining, 2×10^5 cells were diluted in 100 μl of FACS buffer (PBS (pH7.4), 0.1% BSA, 0.02% NaN_3) and were treated for 10 min at 4°C with normal mouse Ig (Sigma-Aldrich) or mouse FcγR-specific 2.4G2 Ab to block unspecific binding or binding to Fc receptors. Subsequently, cells were stained for 30 min with labeled mAbs, washed, and stained with another mAb or analyzed with a FACScan or FACSCalibur flow cytometer (BD Biosciences).

All mouse and rat mAbs were obtained from BD Pharmingen and are given with their clone names: mouse Vβ8.1, 8.2, 8.3 (F23.1); mouse CD3 ε-chain (145-C11); mouse CD1d (1B1); mouse CD4 (GK1.5); mouse CD8α (53-6.7); NK1.1 (PK136); BV8S4A1 and BV8S4A2, Vβ8.2 of LEW rats and Vβ8.4 of F344/Crl rat (R78); rat TCR β-chain (R73); rat CD4 (W3/25); rat CD4 (OX35); rat CD8β (3.4.1.); rat NKR-P1A (10-78). Abs were usually FITC or PE labeled. Biotinylated mAbs, when used, were visualized with streptavidin-CyChrome. Unconjugated Abs, used in indirect immunofluorescent staining, were detected by using fluorochrome-conjugated Abs: PE- or Cy5.5-conjugated $(Fab')_2$ fragment of donkey anti-mouse IgG or goat anti-hamster IgG FITC obtained from Dianova or Serotec).

Staining with α-GalCer-loaded mouse CD1d-PE tetramer

α-GalCer-loaded or control mouse CD1d-PE tetramers were generated as described in Ref. 18. Tetramer staining of mouse/rat IHL- or TCR-transduced cell lines was performed as normal FACS staining, but with incubation for 1 h at room temperature. Tetramer concentrations were 350 (high tetramer) or 35 ng/50 μl cell suspension (low tetramer).

Results

Phenotype and α-GalCer response of rat IHL

In mouse and human, the highest proportion iNKT cells can be found among intrahepatic lymphocytes. In an attempt to identify the corresponding population in rat, IHL of F344/Crl rats and C57BL/6 mice were compared for cell surface phenotype (Fig. 1*A*), binding of α-Gal-loaded mouse CD1d tetramers (Fig. 1*B*), and α-GalCer-induced cytokine production (Fig. 1*C*). In agreement with published data, about one-third of mouse IHL coexpressed NK1.1 (mouse homolog to rat NKR-P1A) and TCR. More than 20% of IHL coexpressed NK1.1 and CD4, but very few coexpressed NK1.1 and CD8αβ. As shown in Fig. 1*B*, ~27% of IHL show costaining of α-GalCer-loaded CD1d tetramer and anti-CD3, with the tetramer positive cells having a lower or intermediate level of expression of CD3. 25.5% of IHL were costained by tetramer and anti-NK1.1 (data not shown) and 20.4% by tetramer and anti-CD4, whereas only very few (0.38%) stained with CD1d tetramer and CD8-specific mAb (data not shown).

The phenotypes of rat and mouse IHL differed considerably. First of all, <5% of rat IHL coexpressed NKR-P1A and CD3, and most of these cells were positive for CD8αβ but not for CD4, and they did not express intermediate CD3 levels. Secondly, in contrast to results found in mice, only a very small number of $CD3^+$ rat IHL were stained with α-GalCer-loaded mouse CD1d tetramer;

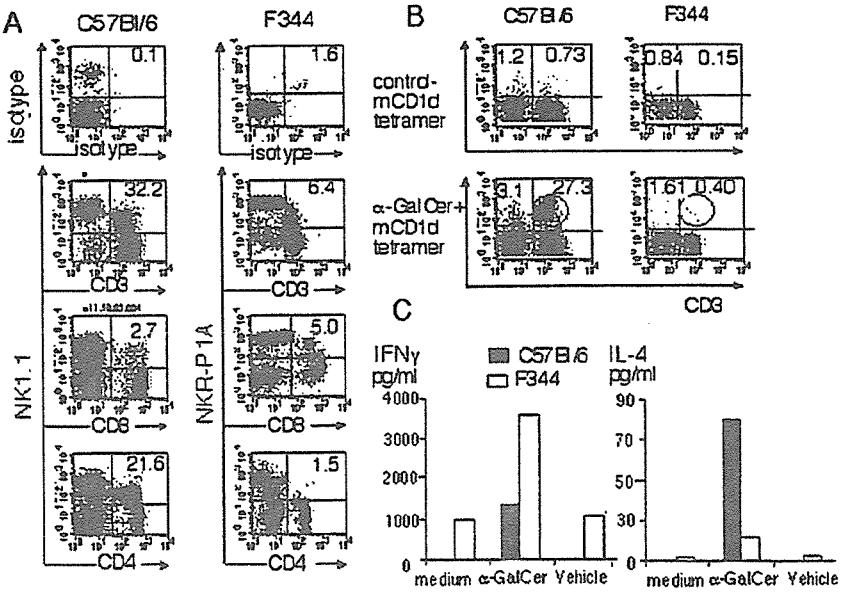

FIGURE 1. Phenotypic and functional analysis of typical iNKT cell features of C57BL/6 mouse and F344/Crl rat IHL. *A*, Two-color flow cytometry for coexpression of NK1.1 or NKR-P1A and indicated T cell markers. Percent of positive cells are indicated by numbers in the *upper right quadrant*. *B*, Two-color flow cytometry for binding of α-GalCer-loaded or unloaded mouse CD1d tetramers to $CD3^+$ positive (*upper right quadrant*) or $CD3^-$ (*upper left quadrant*) C57BL/6 mouse or F344/Crl rat IHL. Percentages of tetramer-positive cells are given in the respective quadrants. *C*, IFN-γ or IL-4 secretion during 24-h stimulation of 1×10^5 rat or mouse IHL with 100 ng/ml α-GalCer dissolved in DMSO, vehicle (DMSO alone), or medium alone. *Ordinate*, Cytokine concentration in picograms per milliliter.

0.4% of IHL were stained with α-GalCer-loaded tetramer and 0.15% with control tetramer. Even higher proportions of $CD3^+$ lymphocytes were stained by α-GalCer-loaded tetramers (1.61%) or control tetramers (0.84%), which made it likely that (much of) the tetramer staining of $CD3^+$ rat IHL was unspecific.

To test whether the lack of binding of mouse CD1d tetramer to rat IHL was due to the absence of α-GalCer-specific cells in F344/Crl rat liver, the α-GalCer reactivity of F344/Crl and C57BL/6 IHL (Fig. 1*C*) was compared. After 24 h of stimulation with α-GalCer (100 ng/ml), mouse and rat liver lymphocytes produced both IFN-γ and IL-4. The amount of rat IL-4 reached ~15% of that secreted by mouse cells. The IFN-γ production by rat IHL exceeded that of mouse IHL, but rat IHL showed also a high level of background IFN-γ production.

The α-GalCer-induced activation of cytokine production in conjunction with the detection of AV14AJ18 rearrangements in rat IHL strongly support the existence of an iNKT cell population in F344/Crl rats, although these cells could not be detected by mouse CD1d tetramer. This could be a consequence of 1) an extremely low frequency of rat iNKT cells and/or 2) a requirement for presentation of α-GalCer by syngeneic CD1d (species specificity), which finally would result in a lack of binding of mouse CD1d tetramers to rat iNKT TCR. To test the latter hypothesis, iNKT TCRs were cloned and expressed in TCR-negative BW58r/mCD28 cells and tested for mouse CD1d tetramer binding. In addition, these lines as well as lines expressing iNKT TCR variants were tested for reactivity to α-GalCer presented by mouse or rat CD1d.

Cloning and transduction of mouse and rat CD1d and iNKT TCR

Cloning, transduction, and quantification of surface expression of iNKT TCR was performed as described in *Materials and Methods*. Three AV14 α-chains were cloned into a retroviral vector carrying an *EGFP* as reporter gene. Two of them comprised V-encoded amino acid sequences identical with that of rat AV14S1 and rat AV14S8. The mouse AV14S1A2-chain was cloned from the α-GalCer-reactive mouse C57BL/6-derived iNKT cell hybridoma KT12. All AV14 α-chains were coexpressed with different mouse or rat BV8S2 β-chains, the properties of which will be discussed later in this section.

The sequences of the tested iNKT TCR α-chains are compared in the upper part of Fig. 2. Both rat AV14S1 and rat AV14S8 α-chain comprise type 1 AV14 sequences. The V domain of the rat AV14S1 α-chain is identical with sequences previously found by Matsuura et al. in F344/Crl rat liver (6). The rat AV14S8 α-chain sequence was directly cloned from F344/Crl IHL, as described in *Materials and Methods*. AV14S8 has not yet been described for F344/Crl rats, but an identical sequence has been found in the BN/SsNHsd rat genome, where it has been named AV14S8 (25). A peculiarity of the AV14S8-comprising α-chain used in this study may be the valine located at position 93 of the VJ junction which corresponds to the adult type of AV14AJ18 rearrangements (26). Otherwise, the mature Vα domains of the two rat TCRs differed by the following substitutions: K1R, Q15E, and K51T.

The middle part of Fig. 2 aligns the sequences of the TCR β-chains used in this study. The BV8S2-positive mouse β-chain was originally isolated from the iNKT T cell hybridoma KT12. The rat BV8S2 (BV8S2A1 or Tcrb-V8.2[1])-comprising β-chain used in this study was derived from the rat T cell hybridoma 35/1, which was generated with an encephalitogenic cell line of LEW/Crl origin as fusion partner. The 35/1 TCR is RT1B[1]-restricted $gpMBP_{68-88}$ specific and reacts also with the superantigens of *Yersinia pseudotuberculosis* and *Mycoplasma arthritidis* and the staphylococcal enterotoxins B and C1 (33). As previously described in some detail (33), replacement of the CDR2 and/or the CDR4/HV4 of the BV8S4A2 with those of F344/Crl rats had distinct effects on (super)Ag reactivity. Changes in the CDR2 abolished reactivity for peptide Ag and staphylococcal enterotoxins B and C1, whereas mutation of the HV4/CDR4 affected only the response to staphylococcal enterotoxins (33). The β-chain containing the mutations within CDR2 and CDR4 is, with exception of a lacking L14K substitution, identical with the BV8S4A2 of F344/Crl rats. It lost specificity for the peptide Ag, staphylococcal enterotoxins and the superantigen of *M. arthritidis* (33).

The lower part of Fig. 2 presents the amino acid sequence of the α-1 and α-2 domains of rat and mouse CD1d. The α-helical parts

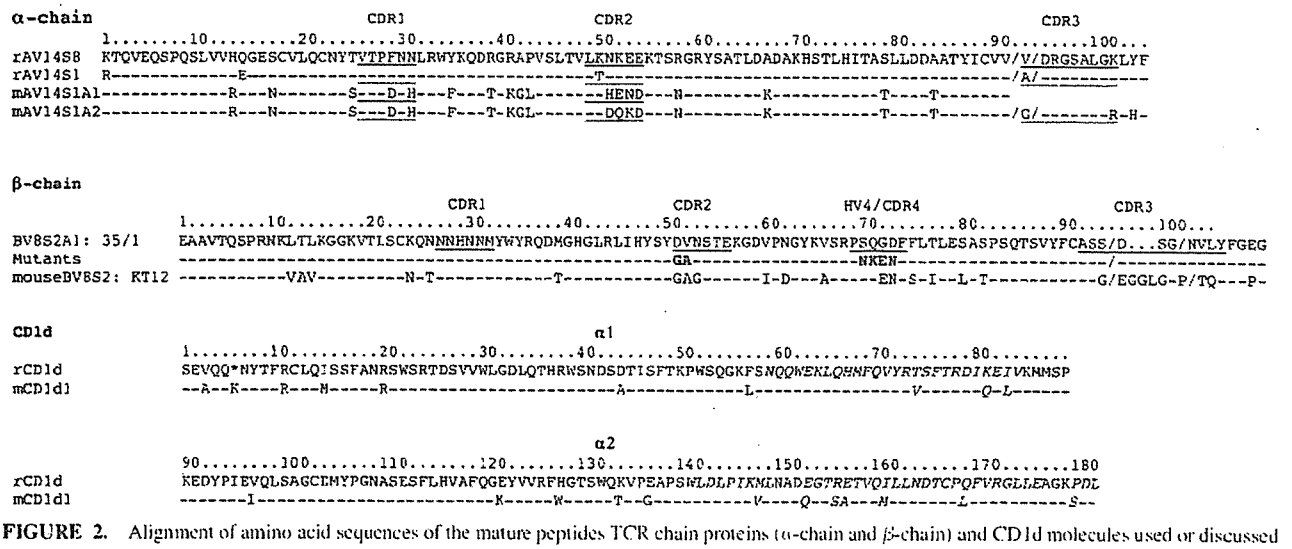

FIGURE 2. Alignment of amino acid sequences of the mature peptides TCR chain proteins (α-chain and β-chain) and CD1d molecules used or discussed in this study. Underlined parts of the TCR sequences indicate localization of CDRs. Parts of CD1d sequences in italics indicate α-helical regions. Amino acid sequences were deduced from the nucleotide sequences, the accession numbers of which can be found in GenBank: rAV14S8 α-chain, DQ340291; rAV14S1 α-chain, DQ340293; mAV14S1, AY158221; mAV14S1A2 (KT12 hybridoma), DQ340292; BV8S2A1 TCR35/1 β-chain, AY228549. Mutants entry indicates localization of the CDR2 and CDR4/HV4 substitutions introduced in the TCR35/1 β-chain, which are highlighted by bold letters. mBV8S2 TCR KT12, DQ340294; mCD1d (mouse CD1d), X13170.1; rCD1d (rat CD1d), AB029486.

of CD1d are marked. The α helices of the α1 domains differ in 3 aa. Visualization of the of the PDB files 1ZHN (10) and 1Z5L (12) of the mouse CD1d crystal structure by Swiss-PDB-viewer (http://swissmodel.expasy.org/SM_TOPPAGE.html) shows that T74 points upwards and K81 outwards, defining them as theoretical contact sites with the TCR. I83 points into the binding groove. The α-helical parts of the α-2 domain differ by 7 aa. With exception of the R157S, side chains of all substitutions show upwards and provide possible contacts for the TCR. In contrast to the differences in potential TCR contacts, those amino acids shown to provide H bonds with α-GalCer are conserved (12). Both *CD1d* genes were expressed in P815 cells (P80rCD80) overexpressing rat CD80 as described in *Materials and Methods*.

Species specificity of CD1d restriction in Ag recognition by rat iNKT TCR

First, we tested three responder cell lines for their α-GalCer reactivity and their capacity to bind mouse CD1d tetramers. The lines were BWr/mCD28 cells expressing: 1) as positive control, mouse iNKT TCR isolated from the KT12 hybridoma which consisted of a mouse AV14S1A2 α-chain and mouse BV8S2 β-chain; 2) rat AV14S1 α-chain with the CDR2+4 β-chain mutant; 3) the rat AV14S8 α-chain with the same β-chain mutant. The BV8S4-like CDR2+4 β-chain mutant was used, because there is circumstantial evidence that in F344/Crl rats, iNKT cells express the BV8S4-comprising β-chains (6). The two rat TCR lines expressed very similar levels of TCR, whereas expression of the mouse TCR was considerably lower (Fig. 3). Cell lines were tested three to five times for their α-GalCer-induced IL-2 secretion. IL-2 levels after CD3 ligation were quite similar, with the exception of sometimes considerably lower IL-2 production by the mouse iNKT TCR-transduced line (data not shown). Fig. 3 shows data from one representative assay of α-GalCer-induced IL-2 secretion. The APC-type thymocytes vs CD1d-transduced P80 cells and the origin of the transduced CD1d (rat vs mouse) considerably affected the outcome of the assay. Generally, with CD1d-transduced P80rCD80 cells as APC, IL-2 production was much higher than with thymocytes. This may reflect the differences in the level of CD1d and CD80 surface expression in primary vs CD1d-transduced cells (data not shown). In assays with mouse thymocytes as APC, some background IL-2 production was found, even if TCR-negative BW58 cells were used as responders, suggesting that IL-2 was secreted by α-GalCer-stimulated thymocytes (Figs. 3 and 5). With regard to a possible species specificity in CD1d-restricted α-GalCer recognition, all three lines responded to α-GalCer presented by rat CD1d-expressing cells, whereas α-GalCer mouse CD1d complexes stimulated only mouse iNKT TCR responder cells. In addition, the stimulation of the line expressing the rat AV14S1 α-chain was considerably stronger than of the rat AV14S8 α-chain-expressing line.

The differences in the response to α-GalCer presented by mouse CD1d correlated with the pattern of mouse CD1d tetramer staining as is shown in Fig. 3. Binding of mouse CD1d tetramers was normalized by dividing mean fluorescence intensity (MFI) of tetramer staining, through MFI of CD3 staining. After normalization, tetramer staining of the mouse iNKT TCR-expressing line was 24-fold, respectively, 8-fold stronger than that of the rat AV14S8 α-chain-expressing line or the rat AV14S1 α-chain-expressing line.

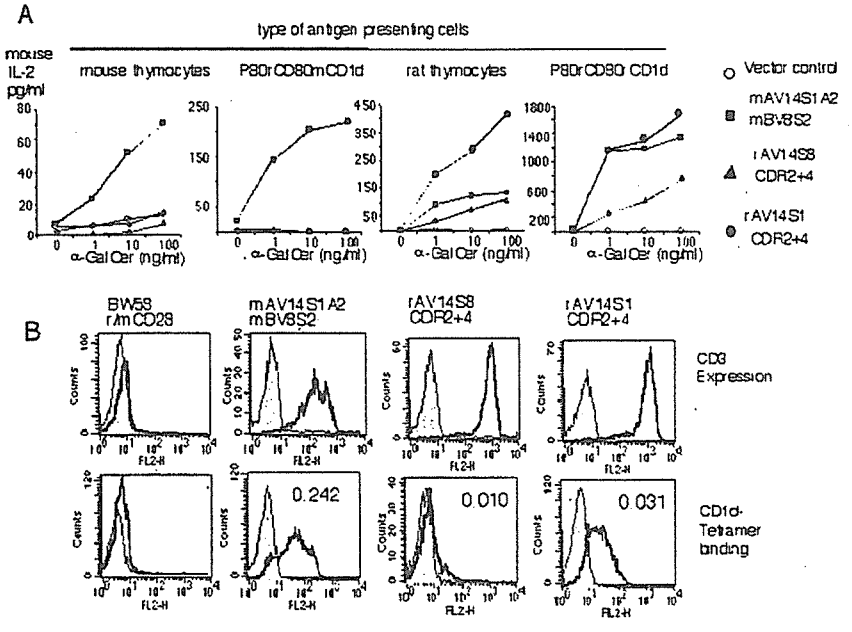

FIGURE 3. *A*, Species specificity of CD1d-restricted α-GalCer recognition by rat iNKT TCR-transduced cells. The graphs in the upper row indicate degree of IL-2 production (please note the different scales of the ordinates) by TCR-transduced BW58r/mCD28 cells after stimulation with α-GalCer presented by different APC-expressing mouse or rat CD1d. Transduced TCR: ○, vector control; ■, mAV14S1A2+ mBV8S2 (mouse α-chain + mouse β-chain); ▲, AV14S8 + rat CDR2+4 β-chain (rat AVS8 α-chain + BV8S4-like rat β-chain); ●, AV14S1 + rat CDR2+4 β-chain (rat AVS1 α-chain + BV8S4-like rat β-chain). Amino acid sequences of the TCR chains used by these are given in Fig. 2. The type of α-GalCer-presenting cells and concentrations of α-GalCer used for stimulation are indicated on top of the respective graphs and at the abscissa, respectively. Zero ng/ml indicates the use of vehicle control. *B*, *Upper row*, CD3 expression of TCR-transduced cell lines used in *A*. Binding of isotype control (▨) or anti-CD3 (▩). *Lower row*, Mouse CD1d tetramer staining. Binding of unloaded control (350 ng/50 μl sample, □) and of α-GalCer-loaded tetramers (350 ng/50-μl sample, ▯). The type of transduced TCR is given on top of the histograms. The numbers in the histogram give ratios of MFIs for staining with α-GalCer-loaded mouse CD1d tetramers divided by that for staining with anti-CD3.

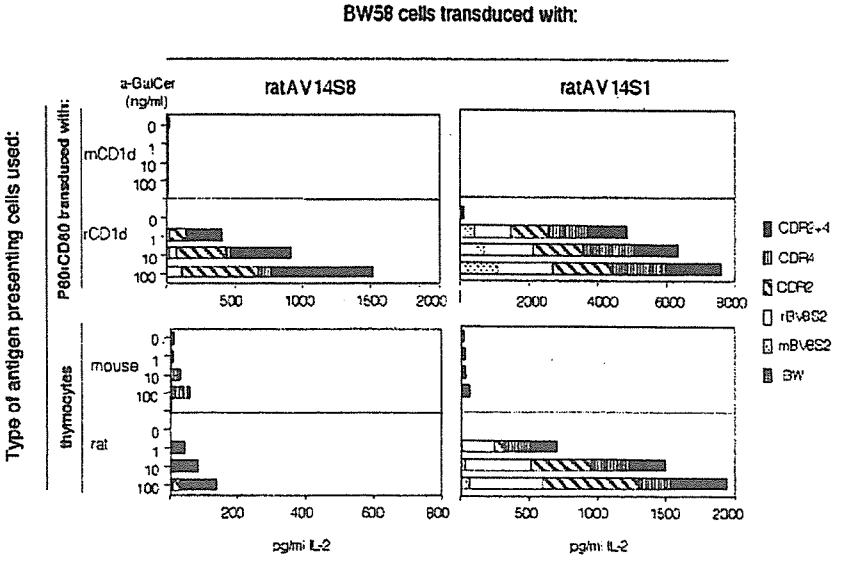

FIGURE 4. CD1d-restricted α-GalCer recognition of rat iNKT TCR. Species specificity of CD1d restriction. Shown is the α-GalCer-induced IL-2 production of BW58r/m CD28 transduced with rat AV14S1 or AV14S8 α-chains and various β-chains and different types of APC. Each section of the column indicates IL-2 production by cells expressing a certain α-β-chain combination. The α-chain is indicated at the top of the graph, the β-chains are indicated by the symbols in the graph. BW, Cells transduced with vector control. Ordinate, Type of APCs and the origin of CD1d. Note the variation of the scales indicating IL-2 production in the various graphs. α-GalCer concentrations are given in nanograms per milliliter. Vehicle designates culture with solvent (DMSO) only.

Effects of iNKT TCR α- and β-chain differences on CD1d-restricted α-GalCer recognition

We have previously analyzed the effects of CDR2 and/or CDR4 mutations of rat BV8S2 on the recognition of peptide Ags and superantigens (33). To learn whether the known BV encoded (super)Ag recognition sites may also contribute to α-GalCer recognition, AV14 α-chains were coexpressed with the various rat BV8S2 β-chain mutants and a mouse BV8S2 β-chain. These lines were then tested for the response to α-GalCer presented either by rat or mouse CD1d and for binding of α-GalCer-loaded mouse CD1d tetramer.

All lines expressed similar levels of TCR (summarized in Fig. 6) and produced similar amounts of IL-2 after stimulation with anti-CD3 mAb, with the exception of the mouse β-chain-expressing lines, which sometimes showed a rather low level of IL-2 production (data not shown). All lines were tested two to five times; and although the overall degree of stimulation varied between experiments, the patterns of α-GalCer reactivity remained the same. Figs. 4 and 5 show results from a representative experiment comparing all cell lines and Fig. 6 summarizes the results of all experiments.

The iNKT TCR composition affected the α-GalCer reactivity as follows: 1) the α-chain sequence of the transduced TCR largely affected the general degree of α-GalCer reactivity, because all rat AV14S1 α-chain-expressing lines responded considerably better to α-GalCer than the corresponding rat AV14S8 α-chain-expressing lines (Figs. 3 and 4); 2) lines with TCR comprising the two rat α-chains showed no or only a marginal response to α-GalCer which was presented by mouse CD1d, regardless of the type of the pairing β-chain (Fig. 4). These findings confirmed and extended the results on the species specificity of CD1d-restricted α-GalCer recognition by rat iNKT TCR shown in Fig. 3) only lines with TCR comprising the mouse α-chain in combination with mouse β-chain or with suitable rat β-chains responded to α-GalCer presented by mouse CD1d (Fig. 5). Suitable were those rat β-chains, which contained the BV8S4-like CDR2 (CDR2 or CDR2+4 mutant), whereas β-chains with the CDR2 of rat BV8S2 (CDR4 mutant and wild-type BV8S2) showed in the same setting only a marginal or no response. This pattern of reactivity maps the CDR2 of the β-chain as a region contributing to CD1d-restricted α-GalCer recognition in the interspecies comparison.

In contrast to the variation in the response to α-GalCer presented by mouse CD1d, recognition of rat CD1d-α-GalCer complexes was largely unaffected by the β-chain of iNKT TCR. All lines expressing TCR comprising the rat or mouse AV14S1 α-chains (Figs. 4 and 5) showed a very similar response. The

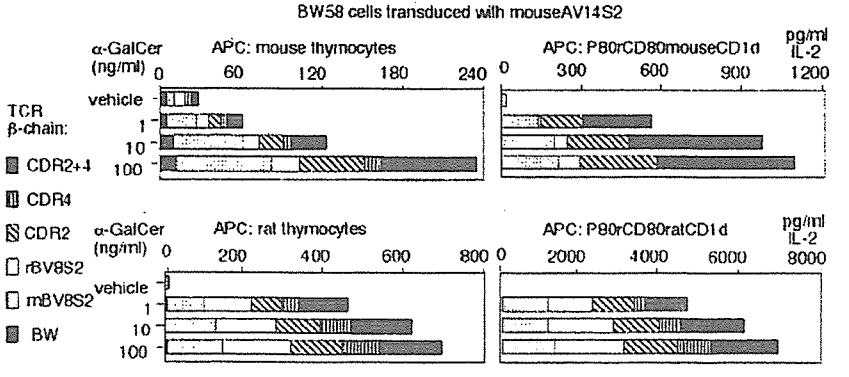

FIGURE 5. Analysis of mouse CD1d restricted α-GalCer recognition by chimeric mouse α- rat-β-chain iNKT TCR reveals contribution of CDR2β to ligand recognition by iNKT TCR. Shown is IL-2 production of BW58r/m CD28 transduced with AV14S1A2 α-chains and various β-chains indicated by the symbols in the graph to α-GalCer presented by indicated APC. BW indicates cells transduced with vector control. Every section of the columns indicates IL-2 production by cells expressing a certain α-β-chain combination. Note the variation of the scales indicating IL-2 production in the various graphs. α-GalCer concentrations are given in ng/ml. Vehicle designates culture with solvent (DMSO) only.

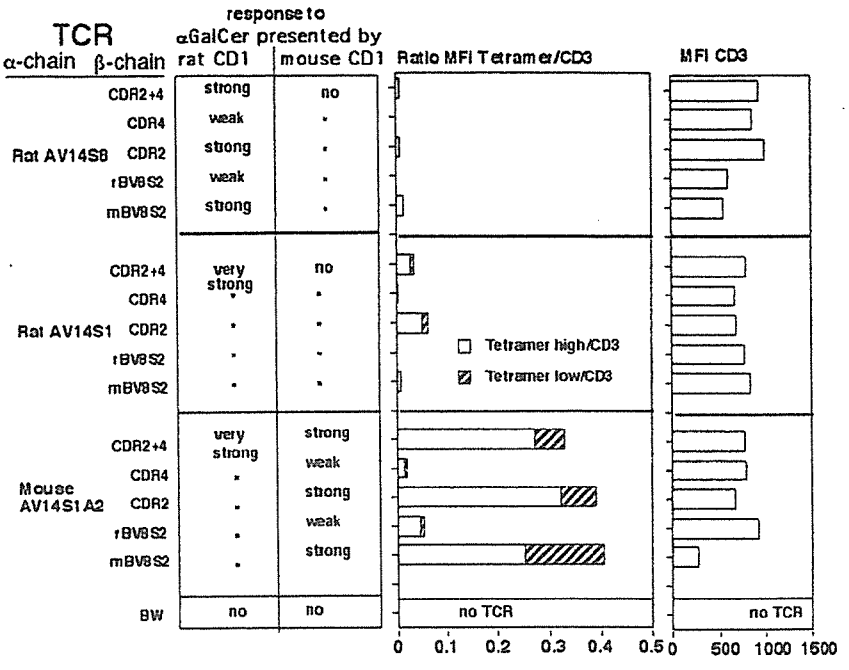

FIGURE 6. Survey of α-GalCer responsiveness of TCR-transduced cell lines, their CD1d tetramer binding, and TCR expression. The left part of the figure summarizes functional data of three to five experiments on the response to α-GalCer presented by rat or mouse CD1d by cell lines expressing the indicated iNKT TCR combinations (see also Figs. 3–5). The central part gives an estimate on CD1d tetramer binding for different cell lines. The stacked bars depict the ratio of MFIs obtained by staining with 350 ng (tetramer high) or 35 ng (tetramer low) of CD1d tetramer divided by the MFI of anti-CD3 staining. Numbers on the abscissa indicate this ratio. Examples for the staining are given in Fig. 3. The right part gives the MFI of CD3 staining of the cell lines used to generate of the data depicted in the central part of the graph.

somewhat lower IL-2 production of the line coexpressing rat AV14S1 α-chain and the CDR4 mutant β-chain probably reflects a generally weaker capacity in TCR-triggered IL-2 production, because anti-CD3 induced IL-2 secretion (not shown) was only about one-half of that found for the other lines. Less clear were the results for cell lines expressing rat AV14S8 α-chain. In two of four experiments, β-chain composition affected the response to rat CD1-α-GalCer complexes of the lines. An example for such a differential response is given in Fig. 4, where the lines expressing the CDR2 or CDR2+4 mutant β-chains reacted far better than those lines expressing the wild-type BV8S2 or the CDR4 mutant.

Finally, effects of the α-chain composition were also seen for the three mouse β-chain-expressing lines. The rat AV14S8 α-chain/mouse β-chain-expressing line completely lacked α-GalCer reactivity (Fig. 4), whereas the rat AV14S1 α-chain/mouse β-chain expressing line responded to α-GalCer if it was presented by rat CD1d-transduced P80rCD80 cells (Fig. 4), implicating rat Vα interactions with CD1d in imparting the observed species specificity. Only the mouse AV14S1A2 α-chain/mouse β-chain expressing line responded irrespective of the types of APC or origin of CD1d used to present the α-GalCer (Fig. 4).

Differential binding of α-GalCer-loaded mouse CD1d tetramers to iNKT-TCR-transduced lines

All cell lines were also tested for TCR expression and binding of α-GalCer-loaded tetramers at two different concentrations. In all cases, binding of unloaded tetramer control was negligible. Fig. 6 summarizes data from such an experiment and gives an overview of the results obtained in the functional assays. The capacity to bind α-GalCer-loaded mouse CD1d tetramers is presented by the ratio of MFI of tetramer binding and MFI of anti-CD3 binding. The best binding was found for the TCR comprising mouse AV14S1 α-chain paired with the CDR2, CDR2+4 mutants of rat BV8S2 β-chains or the mouse BV8S2 β-chain (Figs. 3 and 6), which is consistent with their exclusive capacity to respond to α-GalCer presented by mouse CD1d. At least 8 times weaker was the tetramer binding of lines coexpressing mouse α-chains and rat BV8S2 and CDR4 mutants.

Interestingly, the tetramer binding varied also between the rat α-chain-expressing lines. The poorly responding rat AV14S8 α-chain-expressing lines showed essentially no binding, whereas at least some tetramer binding was found for the more reactive lines coexpressing rat AV14S1 α-chain and the suitable CDR2 or CDR2+4 mutated β-chains. Finally, and again consistent with the functional assays, the rat α-chains paired with mouse β-chain bound no tetramer, whereas the original mouse iNKT TCR bound it very well. Indeed, the efficient binding of this TCR at the lower tetramer concentration suggests a rather high avidity of the original mouse iNKT TCR for α-GalCer-mouse CD1d complexes, consistent with measurements conducted with other mouse iNKT cell hybridomas and T cell populations.

Fig. 6 summarizes our results on the CD1d-restricted α-GalCer response and binding of α-GalCer-loaded mouse CD1d tetramers to iNKT TCR-transduced cell lines. It appears that the lack of reactivity to α-GalCer presented by mouse CD1d results from an impaired binding of the rat iNKT TCR α- rather than β-chain to mouse CD1d. Furthermore, comparison of iNKT TCR sharing the same α-chain but comprising different β-chains revealed that the amino acid composition of CDR2 of the β-chain strongly affects the CD1d-restricted glycolipid reactivity.

Discussion

This study was initiated to characterize the phenotype and the α-GalCer response of rat iNKT cells in a side by side comparison of mouse and rat IHL. As previously described (1, 6, 28), ~30% of mouse IHL coexpressed NK1.1 and TCR and were either $CD4^+$ or $CD4^-CD8^-$, whereas rat IHL comprised rather low numbers of NKR-P1A (rat homolog of NK1.1) and TCR^+ cells, most of them being $CD8\alpha\beta^+$. Our attempts to directly detect rat iNKT cells by staining with α-GalCer-loaded mouse CD1d tetramers failed, although the capacity of rat IHL to produce IFN-γ and IL-4 production after stimulation with α-GalCer suggested that there is indeed a functional iNKT cell population in F344/Crl rats. Analysis of newly generated cell lines expressing CD1d and iNKT TCR of both species allowed us to directly demonstrate the functionality of the rat elements of cognate Ag recognition by iNKT cells. In

addition, this analysis revealed that Ag recognition by rat iNKT TCR required its presentation by syngeneic CD1d, which was unexpected, given that mouse and human CD1d tetramers and dimers (18–20) bind to iNKT cells of the opposite species. Nevertheless, despite this cross-species reactivity, mouse iNKT TCRs bind mouse CD1d better than human CD1d, as was shown with α-GalCer-loaded mouse CD1d dimers (4). In addition, the weakly binding human dimers showed a stronger preference for mouse BV8S2 iNKT TCR than for mouse dimers, a result that underlines the substantial contribution of the β-chain to binding of α-GalCer CD1d complexes (4).

Interestingly, mouse iNKT TCR-transduced lines responded quite well to α-GalCer presented by rat and by mouse CD1d, whereas the rat iNKT TCR-expressing lines responded only when Ag was presented by rat CD1d. What could be the reason for the need of syngenicity between iNKT TCR and CD1d only in one direction? One possibility could be that higher numbers of α-GalCer complexes on rat $CD1d^+$ APCs could have compensated for the generally low avidity of rat iNKT TCR for CD1d, in particular for mouse CD1d. This possibility cannot be formally excluded but seems to be rather unlikely because homologous types of APC were used for presentation. Alternatively, we suggest a higher degree of promiscuity either in Ag recognition by mouse vs rat iNKT TCR or in Ag presentation by rat vs mouse CD1d.

With the help of chimeric and mutated iNKT TCR, we could identify TCR regions, which contribute to binding of α-GalCer and (mouse) CD1d. Cell lines expressing TCR comprising a mouse iNKT TCR α-chain and a suitable β-chain transgressed the threshold for the induction of a response to Ags presented by mouse CD1d, and these cells efficiently bound mouse CD1d tetramers. The differential reactivity of the rat BV8S2 β-chain mutants allowed us for the first time to demonstrate the important role of BV-encoded parts in the α-GalCer response, without a possible interference by CDR3 diversity. In addition, analysis of mutants swapping the CDR2 of BV8S2 with that of BV8S4 provided evidence for an involvement of the CDR2 of the β-chain in recognition of the α-GalCer-CD1d complex. In this context, it is of interest that the CDR2 of rat BV8S4, which in the combination with the mouse iNKT TCR α-chain permitted binding of α-GalCer-mouse CD1d complexes, and the CDR2 of mouse BV8S differ from each other by only one amino acid (Fig. 2). In contrast, the CDR2 of rat BV8S2, which in the interspecies comparison was nonpermissive, differed from that of mouse BV8S2 by 3 aa.

Rat *Tcrb* haplotypes vary in expression of functional BV8S2 and BV8S4 genes. The *Tcrb*^{a} haplotype, which is found in F344/Crl and DA rats, expresses BV8S2 and BV8S4, whereas the *Tcrb*^{l} haplotype of LEW/Cr, BN, and PVG rats expresses only BV8S2 (24, 31, 41, 42). These rat strains are widely used as models for autoimmune diseases; therefore, it is of special interest to investigate whether differences in reactivity to natural iNKT TCR ligands based on differences in the CDR2s of BV8S2 vs BV8S4 could lead to a rat strain-specific variation in iNKT T cell development or Ag reactivity.

The three α-chains tested contributed not only to restricted recognition of syngeneic CD1d, but also to the overall magnitude of the α-GalCer response. The lines expressing TCR with rat AV14S1 chains and mouse AV14S1A2 α-chains showed a much better response than the rat AV14S8-expressing lines. By analogy to what is known from MHC-restricted recognition of peptide Ags, the differences in α-GalCer reactivity of the two rat α-chains could have been explained by the K50T substitution in the CDR2α and by the A93V difference in the CDR3α (43). Two reasons lead us to assume that the CDR2α difference is of minor importance. In a comprehensive study on a mouse AV14S1 polymorphism, Sim et al. (44) demonstrated that a pronounced CDR2α difference between mouse AV14S1A1 and AV14S1A2 (see also Fig. 2) had little if any effect on TCR-binding to α-GalCer-CD1d complexes (44). Also, our own preliminary results (E. Pyz, I. Müller, and T. Herrmann, unpublished observations) obtained with rat AV14S1 and AV14S8 chain mutants showed little effect of the K50T substitution on the α-GalCer response, whereas a pronounced effect was found for the V93A substitution.

To sum up, we showed that efficient activation of rat iNKT TCR-expressing lines requires presentation of α-GalCer by syngeneic CD1d, and that reactivity to complexes of α-GalCer and mouse CD1d can be obtained by replacing the rat α-chain against that of the mouse and by using a β-chain comprising the CDR2 of rat BV8S4.

This finding thus provides the first description of a germline-encoded CDR involved in ligand recognition by iNKT TCR. The generation and functional analysis of further chimeric rat/mouse iNKT TCR and of chimeric rat/mouse CD1d molecules should strongly facilitate the characterization of the TCR/CD1d/Ag complex. At a certain point of chimerism of TCR or CD1d, cells expressing iNKT TCR comprising rat/mouse α-chain chimeras would be expected to gain specificity for α-GalCer presented by mouse CD1d and mouse/rat CD1d chimeras should gain the capacity to efficiently present Ag to rat iNKT TCR. Finally, combined functional assays with cells expressing such chimeric or mutated receptors and ligands, at best together with binding studies of recombinant molecules, may even allow definition of direct contacts in the ternary complex comprising iNKT TCR/Ag and CD1d.

Acknowledgments

We thank Kathrin Krejci and Ingrid Müller for excellent technical assistance and Niklas Beyersdorf and Barabara Sullivan for critical reading of the manuscript.

Disclosures

The authors have no financial conflict of interest.

References

1. Godfrey, D. I., H. R. MacDonald, M. Kronenberg, M. J. Smyth, and L. Van Kaer. 2004. NKT cells: what's in a name? *Nat. Rev. Immunol.* 4: 231–237.
2. Lantz, O., and A. Bendelac. 1994. An invariant T cell receptor α chain is used by a unique subset of major histocompatibility complex class I-specific $CD4^+$ and $CD4-8^-$ T cells in mice and humans. *J. Exp. Med.* 180: 1097–1106.
3. Matsuda, J. L., L. Gapin, N. Fazilleau, K. Warren, O. V. Naidenko, and M. Kronenberg. 2001. Natural killer T cells reactive to a single glycolipid exhibit a highly diverse T cell receptor β repertoire and small clone size. *Proc. Natl. Acad. Sci. USA* 98: 12636–12641.
4. Schumann, J., R. B. Voyle, B. Y. Wei, and H. R. MacDonald. 2003. Cutting edge: influence of the TCR Vβ domain on the avidity of CD1d:α-galactosylceramide binding by invariant Vα14 NKT cells. *J. Immunol.* 170: 5815–5819.
5. Dellabona, P., E. Padovan, G. Casorati, M. Brockhaus, and A. Lanzavecchia. 1994. An invariant Vα24-JαQ/Vβ 11 T cell receptor is expressed in all individuals by clonally expanded $CD4-8^-$ T cells. *J. Exp. Med.* 180: 1171–1176.
6. Matsuura, A., M. Kinebuchi, H. Z. Chen, S. Katabami, T. Shimizu, Y. Hashimoto, K. Kikuchi, and N. Sato. 2000. NKT cells in the rat: organ-specific distribution of NKT cells expressing distinct Vα14 chains. *J. Immunol.* 164: 3140–3148.
7. Swann, J., N. Y. Crowe, Y. Hayakawa, D. I. Godfrey, and M. J. Smyth. 2004. Regulation of antitumour immunity by CD1d-restricted NKT cells. *Immunol. Cell Biol.* 82: 323–331.
8. Skold, M., and S. M. Behar. 2003. Role of CD1d-restricted NKT cells in microbial immunity. *Infect. Immun.* 71: 5447–5455.
9. Taniguchi, M., M. Harada, S. Kojo, T. Nakayama, and H. Wakao. 2003. The regulatory role of Vα14 NKT cells in innate and acquired immune response. *Annu. Rev. Immunol.* 21: 483–513.
10. Giabbai, B., S. Sidobre, M. D. Crispin, Y. Sanchez-Ruiz, A. Bachi, M. Kronenberg, I. A. Wilson, and M. Degano. 2005. Crystal structure of mouse CD1d bound to the self ligand phosphatidylcholine: a molecular basis for NKT cell activation. *J. Immunol.* 175: 977–984.
11. Koch, M., V. S. Stronge, D. Shepherd, S. D. Gadola, B. Mathew, G. Ritter, A. R. Fersht, G. S. Besra, R. R. Schmidt, E. Y. Jones, and V. Cerundolo. 2005. The crystal structure of human CD1d with and without α-galactosylceramide. *Nat. Immunol.* 6: 819–826.

12. Zajonc, D. M., C. Cantu, 3rd, J. Mattner, D. Zhou, P. B. Savage, A. Bendelac, I. A. Wilson, and L. Teyton. 2005. Structure and function of a potent agonist for the semi-invariant natural killer T cell receptor. *Nat. Immunol.* 6: 810–818.
13. Zhou, D., J. Mattner, C. Cantu III, N. Schrantz, N. Yin, Y. Gao, Y. Sagiv, K. Hudspeth, Y. Wu, T. Yamashita, et al. 2004. Lysosomal glycosphingolipid recognition by NKT cells. *Science* 306: 1786–1789.
14. Kinjo, Y., D. Wu, G. Kim, G. W. Xing, M. A. Poles, D. D. Ho, M. Tsuji, K. Kawahara, C. H. Wong, and M. Kronenberg. 2005. Recognition of bacterial glycosphingolipids by natural killer T cells. *Nature* 434: 520–525.
15. Mattner, J., K. L. Debord, N. Ismail, R. D. Goff, C. Cantu, 3rd, D. Zhou, P. Saint-Mezard, V. Wang, Y. Gao, N. Yin, et al. 2005. Exogenous and endogenous glycolipid antigens activate NKT cells during microbial infections. *Nature* 434: 525–529.
16. Sandberg, J. K., and H. G. Ljunggren. 2005. Development and function of CD1d-restricted NKT cells: influence of sphingolipids, SAP and sex. *Trends Immunol.* 26: 347–349.
17. MacDonald, H. R. 2000. CD1d-glycolipid tetramers: A new tool to monitor natural killer T cells in health and disease. *J. Exp. Med.* 192: F15–F20.
18. Matsuda, J. L., O. V. Naidenko, L. Gapin, T. Nakayama, M. Taniguchi, C. R. Wang, Y. Koezuka, and M. Kronenberg. 2000. Tracking the response of natural killer T cells to a glycolipid antigen using CD1d tetramers. *J. Exp. Med.* 192: 741–754.
19. Karadimitris, A., S. Gadola, M. Altamirano, D. Brown, A. Woolfson, P. Klenerman, J. L. Chen, Y. Koezuka, I. A. Roberts, D. A. Price, et al. 2001. Human CD1d-glycolipid tetramers generated by in vitro oxidative refolding chromatography. *Proc. Natl. Acad. Sci. USA* 98: 3294–3298.
20. Benlagha, K., A. Weiss, A. Beavis, L. Teyton, and A. Bendelac. 2000. In vivo identification of glycolipid antigen-specific T cells using fluorescent CD1d tetramers. *J. Exp. Med.* 191: 1895–1903.
21. Naidenko, O. V., J. K. Maher, W. A. Ernst, T. Sakai, R. L. Modlin, and M. Kronenberg. 1999. Binding and antigen presentation of ceramide-containing glycolipids by soluble mouse and human CD1d molecules. *J. Exp. Med.* 190: 1069–1080.
22. Ichimiya, S., K. Kikuchi, and A. Matsuura. 1994. Structural analysis of the rat homologue of CD1: evidence for evolutionary conservation of the CD1D class and widespread transcription by rat cells. *J. Immunol.* 153: 1112–1123.
23. Katabami, S., A. Matsuura, H. Z. Chen, K. Imai, and K. Kikuchi. 1998. Structural organization of rat CD1 typifies evolutionarily conserved CD1D class genes. *Immunogenetics* 48: 22–31.
24. Asmuss, A., K. Hofmann, T. Hochgrebe, G. Giegerich, T. Hunig, and T. Herrmann. 1996. Alleles of highly homologous rat T cell receptor β-chain variable segments 8.2 and 8.4: strain-specific expression, reactivity to superantigens, and binding of the mAb R78. *J. Immunol.* 157: 4436–4441.
25. Kinebuchi, M., and A. Matsuura. 2004. Rat T-cell receptor TRAV11 (Vα14) genes: further evidence of extensive multiplicity with homogeneous CDR1 and diversified CDR2 by genomic contig and cDNA analysis. *Immunogenetics* 55: 756–762.
26. Shimamura, M., J. Miura-Ohnuma, and Y. Y. Huang. 2001. Major sites for the differentiation of Vα14$^+$ NKT cells inferred from the V-J junctional sequences of the invariant T-cell receptor α chain. *Eur. J. Biochem.* 268: 56–61.
27. Brissette-Storkus, C., C. L. Kaufman, L. Pasewicz, H. M. Worsey, R. Lakomy, S. T. Ildstad, and W. H. Chambers. 1994. Characterization and function of the NKR-P1dim/T cell receptor-$\alpha\beta^+$ subset of rat T cells. *J. Immunol.* 152: 388–396.
28. Badovinac, V., C. Boggiano, V. Trajkovic, A. B. Frey, N. L. Vujanovic, D. P. Gold, M. Mostarica-Stojkovic, and S. Vukmanovic. 1998. Rat NKR-P1$^+$CD3$^+$ T cells: selective proliferation in interleukin-2, diverse T-cell-receptor-Vβ repertoire and polarized interferon-γ expression. *Immunology* 95: 117–125.
29. Kinebuchi, M., A. Matsuura, K. Ohya, W. Abo, and J. Kitazawa. 2005. Contribution of Vα24Vβ11 natural killer T cells in Wilsonian hepatitis. *Clin. Exp. Immunol.* 139: 144–151.
30. Knudsen, E., T. Seierstad, J. T. Vaage, C. Naper, H. B. Benestad, B. Rolstad, and A. A. Maghazachi. 1997. Cloning, functional activities and in vivo tissue distribution of rat NKR-P1$^+$ TCRαβ$^+$ cells. *Int. Immunol.* 9: 1043–1051.
31. Herrmann, T., K. Hofmann, N. E. Nagel, A. Asmuss, T. Hunig, and K. Wonigeit. 1999. Differential CD4/CD8 subset-specific expression of highly homologous rat Tcrb-V8 family members suggests a role of CDR2 and/or CDR4 (HV4) in MHC class-specific thymic selection. *Int. Immunol.* 11: 435–444.
32. Emoto, M., Y. Emoto, and S. H. Kaufmann. 1995. IL-4 producing CD4$^+$ TCR αβ in liver lymphocytes: influence of thymus, β_2-microglobulin and NK1.1 expression. *Int. Immunol.* 7: 1729–1739.
33. Kreiss, M., A. Asmuss, K. Krejci, D. Lindemann, T. Miyoshi-Akiyama, T. Uchiyama, L. Rink, C. P. Broeren, and T. Herrmann. 2004. Contrasting contributions of complementarity-determining region 2 and hypervariable region 4 of rat BV8S2$^+$ (Vβ8.2) TCR to the recognition of myelin basic protein and different types of bacterial superantigens. *Int. Immunol.* 16: 655–663.
34. Makowska, A., T. Kawano, M. Taniguchi, and S. Cardell. 2000. Differences in the ligand specificity between CD1d-restricted T cells with limited and diverse T-cell receptor repertoire. *Scand. J. Immunol.* 52: 71–79.
35. Kuss, A. W., M. Knodel, F. Berberich-Siebelt, D. Lindemann, A. Schimpl, and I. Berberich. 1999. A1 expression is stimulated by CD40 in B cells and rescues WEHI 231 cells from anti-IgM-induced cell death. *Eur. J. Immunol.* 29: 3077–3088.
36. Lühder, F., Y. Huang, K. M. Dennehy, C. Guntermann, I. Müller, E. Winkler, T. Kerkau, S. Ikemizu, S. J. Davis, T. Hanke, and T. Hünig. 2003. Topological requirements and signaling properties of T cell-activating, anti-CD28 antibody superagonists. *J. Exp. Med.* 197: 955–966.
37. Maeda, K., T. Sato, M. Azuma, H. Yagita, and K. Okumura. 1997. Characterization of rat CD80 and CD86 by molecular cloning and mAb. *Int. Immunol.* 9: 993–1000.
38. Teitell, M., H. R. Holcombe, L. Brossay, A. Hagenbaugh, M. J. Jackson, L. Pond, S. P. Balk, C. Terhorst, P. A. Peterson, and M. Kronenberg. 1997. Nonclassical behavior of the mouse CD1 class I-like molecule. *J. Immunol.* 158: 2143–2149.
39. Bradbury, A., K. T. Belt, T. M. Neri, C. Milstein, and F. Calabi. 1988. Mouse CD1 is distinct from and co-exists with TL in the same thymus. *EMBO J.* 7: 3081–3086.
40. Morita, M., K. Motoki, K. Akimoto, T. Natori, T. Sakai, E. Sawa, K. Yamaji, Y. Koezuka, E. Kobayashi, and H. Fukushima. 1995. Structure-activity relationship of α-galactosylceramides against B16-bearing mice. *J. Med. Chem.* 38: 2176–2187.
41. Torres-Nagel, N. E., T. Herrmann, G. Giegerich, K. Wonigeit, and T. Hunig. 1994. Preferential TCR V usage in rat repertoire selection: Vα8 imparts both positive thymic selection by and alloreactivity to RT1f. *Int. Immunol.* 6: 1367–1373.
42. Stienekemeier, M., K. Hofmann, R. Gold, and T. Herrmann. 2000. A polymorphism of the rat T-cell receptor β-chain variable gene 13 (BV13S1) correlates with the frequency of BV13S1-positive CD4 cells. *Immunogenetics* 51: 296–305.
43. Rudolph, M. G., and I. A. Wilson. 2002. The specificity of TCR/pMHC interaction. *Curr. Opin. Immunol.* 14: 52–65.
44. Sim, B. C., K. Holmberg, S. Sidobre, O. Naidenko, N. Niederberger, S. D. Marine, M. Kronenberg, and N. R. Gascoigne. 2003. Surprisingly minor influence of TRAV11 (Vα14) polymorphism on NKT-receptor mCD1/α-galactosylceramide binding kinetics. *Immunogenetics* 54: 874–883.

doi:10.1093/brain/awl170 Brain (2006), 129, 1984–1992

Selective COX-2 inhibitor celecoxib prevents experimental autoimmune encephalomyelitis through COX-2-independent pathway

Katsuichi Miyamoto,[1,2] Sachiko Miyake,[1] Miho Mizuno,[1] Nobuyuki Oka,[3] Susumu Kusunoki[2] and Takashi Yamamura[1]

[1]Department of Immunology, National Institute of Neuroscience, NCNP, Tokyo, [2]Department of Neurology, Kinki University School of Medicine, Osaka and [3]Department of Rehabilitation Medicine, Minami-kyoto National Hospital, Kyoto, Japan

Correspondence to: Sachiko Miyake, Department of Immunology, National Institute of Neuroscience, NCNP, Kodaira, Tokyo 187-8502, Japan
E-mail: miyake@ncnp.go.jp

Cyclooxygenase (COX) is a key enzyme of arachidonic acid metabolism and exists as two distinct isoforms. COX-1 is constitutively expressed in most tissues, whereas COX-2 is inducibly expressed at the site of inflammation. Selective inhibitors of COX-2 have been developed and have been used as anti-inflammatory agents. Here, we show that a new-generation COX-2 inhibitor, celecoxib, inhibited experimental autoimmune encephalomyelitis (EAE). Celecoxib, but not other COX-2 inhibitors such as nimesulid, prevented myelin oligodendrocyte glycoprotein (MOG) induced EAE when administrated orally on the day of disease induction. Moreover, celecoxib inhibited EAE in COX-2-deficient mice, indicating that celecoxib inhibited EAE in a COX-2-independent manner. In celecoxib-treated mice, interferon-γ (IFN-γ) production from MOG-specific T cells was reduced and MOG-specific IgG1 was elevated compared with vehicle-treated mice. Infiltration of inflammatory cells into the central nervous system and the expression of adhesion molecules, P-selectin and intercellular adhesion molecule-1 (ICAM-1), and a chemokine, monocyte chemoattractant peptide-1 (MCP-1), were inhibited when mice were treated with celecoxib. These results suggest that celecoxib may be useful as a new additional therapeutic agent for multiple sclerosis.

Keywords: COX-2 inhibitor; celecoxib; experimental autoimmune encephalomyelitis; multiple sclerosis

Abbreviations: CMC = carboxymethylcellulose; COX = cyclooxygenase; EAN = experimental autoimmune neuritis; EAE = experimental autoimmune encephalomyelitis; ELISA = enzyme-linked immunosorbent assay; ICAM-1 = intercellular adhesion molecule-1; IFN = interferon; IL = interleukin; LN = lymph node; MCP-1 = monocyte chemoattractant peptide-1; MOG = myelin oligodendrocyte glycoprotein; PBS = phosphate-buffered saline

Received February 6, 2006. Revised April 11, 2006. Accepted May 31, 2006. Advance Access publication July 10, 2006

Introduction

Cyclooxygenase (COX) catalyses the conversion of arachidonic acid to prostaglandins and has two isoforms, COX-1 and COX-2 (Vane *et al.*, 1994; Warner and Mitchell, 2004). COX-1 is constitutively expressed in most tissues and produces prostaglandins involved in maintenance of the gastric mucosa, regulation of renal blood flow and platelet aggregation. On the other hand, COX-2 is inducibly expressed in cells involved in inflammation and in neoplastic tissues by proinflammatory and mitogenic stimuli, and is primarily responsible for the synthesis of prostanoids involved in acute and chronic inflammation (Xie *et al.*, 1997). COX-2 therefore appears to be a suitable target for the anti-inflammatory effects of non-steroidal anti inflammatory drugs. These findings have provided the rationale for the development of selective inhibitors of COX-2.

Celecoxib is a new generation of highly specific COX-2 inhibitors that have been approved for the treatment of rheumatoid arthritis and other inflammatory diseases. The selectivity of COX-2 inhibition is much higher than traditional COX-2 inhibitors (Penning *et al.*, 1997). Furthermore, celecoxib has been shown to exert a potent anti-tumour effect. Interestingly, the anti-tumour effect by celecoxib

has been reported via both COX-2-dependent and COX-2-independent mechanisms (Grosch *et al.*, 2001). For example, cell cycle arrest and apoptosis of various kinds of cells induced by celecoxib appeared to be COX-2-independent effects (Hsu *et al.*, 2000; Arico *et al.*, 2002; Liu *et al.*, 2004).

Experimental autoimmune encephalomyelitis (EAE) is a widely used animal model for multiple sclerosis that can be induced by immunization with myelin antigens such as myelin oligodendrocyte glycoprotein (MOG). EAE is mediated primarily by $CD4^+$ Th1 T cells producing interferon-γ (IFN-γ) and tumour necrosis factor-α (TNF-α) (Nicholson and Kuchroo, 1996; Kumar *et al.*, 1997; Zhang *et al.*, 1997). COX-2 is expressed in neurons and endothelial cells in healthy brain. In rats with EAE, the expression of COX-2 was reported to be upregulated in endothelial cells in inflammatory lesions. In addition, non-selective COX-2 inhibitors have been reported to moderately ameliorate EAE (Prosiegel *et al.*, 1989; Weber *et al.*, 1991; Simmons *et al.*, 1992), suggesting that COX-2 may have an important role in the pathogenesis of EAE (Deininger and Schluesener, 1999). Furthermore, we recently demonstrated that COX-2 inhibitors suppress experimental autoimmune neuritis (EAN), a model of Guillain–Barré syndrome, which is also characterized as a $CD4^+$-Th1 T-cell-mediated autoimmune neurological disease model similar to EAE (Miyamoto *et al.*, 1998, 1999, 2002). These findings led us to investigate the effect of COX-2 inhibitors on EAE.

In the present study, we found that celecoxib greatly suppressed EAE in comparison with traditional COX-2 inhibitors. Furthermore, we have demonstrated that celecoxib inhibited EAE by inhibiting Th1 response of autoreactive T cells and that this inhibition was COX-2-independent. Finally, we demonstrated that celecoxib prevented cell entry into the CNS in association with the inhibition of the expression of P-selectin, intercellular adhesion molecule-1 (ICAM-1) and monocyte chemoattractant peptide-1 (MCP-1). These results highlighted the COX-2-independent therapeutic potential of celecoxib for multiple sclerosis.

Material and methods

Mouse

Wild-type C57BL/6 (B6) mice were purchased from Clea Japan (Tokyo, Japan). COX-2-deficient mice ($COX\text{-}2^{-/-}$) have been backcrossed to B6 background for more than five generations and were purchased from Taconic (Germantown, NY, USA). These mice were maintained under specific pathogen-free conditions.

Induction of EAE

For induction of EAE, mice were immunized (5–10 mice per group) subcutaneously in flanks with 100 μg of MOG_{35-55} peptide (MEVGWYRSPFSRVVHLYRNGK) in 0.1 ml phosphate-buffered saline (PBS) and 0.1 ml complete Freund's adjuvant (CFA) containing 1 mg *Mycobacterium tuberculosis* H37Ra (Difco Laboratories, Detroit, MI, USA) and were injected intravenously with 200 ng of pertussis toxin (List Biological Laboratories, Campbell, CA, USA) on the day of immunization and 2 days later.

Clinical assessment of EAE

EAE was scored on the following scale: 0 = no clinical signs; 1 = partial loss of tail tonicity; 2 = completely limp tail and abnormal gait; 3 = partial hindlimb paralysis; 4 = complete hindlimb paralysis; and 5 = fore- and hindlimb paralysis or moribund state.

Treatment with COX-2 inhibitors

Mice were orally administered 5 μg/g of COX-2 inhibitor, celecoxib (Searle, St Louis, MO, USA) (Penning *et al.*, 1997), nimesulid (Nakarai Tesque, Kyoto, Japan) (Nakatsuji *et al.*, 1996), or indomethacin (Nakarai Tesque) in 0.5% carboxymethylcellulose (CMC) via a feeding cannula every 2 days. Control mice were orally administered vehicle (0.5% CMC) alone.

Measurement of MOG_{35-55}-specific IgG1 and IgG2a titres

Enzyme-linked immunosorbent assay (ELISA) plates (Sumitomo, Tokyo, Japan) were coated with 10 μg/ml MOG_{35-55} in PBS overnight at 4 C. After blocking with 2% bovine serum albumin (BSA) in PBS, different dilutions of the serum from animals at Day 30 after immunization, or normal mice or PBS were added to the plate. MOG_{35-55}-specific antibodies were detected using biotin-labelled anti-IgG1 and anti-IgG2a antibodies (Vector Laboratories, Burlingame, CA, USA). After adding streptavidin-peroxidase (BD Biosciences, San Jose, CA, USA) and a substrate, plates were read at OD_{450} values.

MOG_{35-55}-specific T-cell proliferation assay

On Day 11 after immunization with MOG_{35-55}, draining lymph nodes (LN) were harvested and single cell suspensions were prepared. Cells were cultured in RPMI1640 medium (Gibco, Grand Island, NY, USA) supplemented with 5×10^{-5} M 2-mercaptoethanol, 2 mM L-glutamine, 100 U/ml penicillin and streptomycin and 1% autologous mouse serum, and seeded onto 96-well flat-bottom plates (1×10^6 cells/well). The cells were stimulated with peptide for 72 h at 37 C in a humidified air condition with 5% CO_2. To measure cellular proliferation, [^{3}H]-thymidine was added (1 μCi/well) and uptake of the radioisotope during the final 18 h of culture was counted with a beta-1205 counter (Pharmacia, Uppsala, Sweden). To evaluate proliferative responses of LN cells to peptide, we determined the Δc.p.m. value for cells in each well by subtracting the background c.p.m.

Detection of cytokines and chemokine

LN cells from the MOG_{35-55}-immunized mice were cultured in the standard medium in 96-well flat-bottom plates at 1×10^6/well for 48 h in the presence of the different concentrations of MOG_{35-55}. The concentrations of IFN-γ, interleukin-4 (IL-4) and IL-10 in the supernatants were measured by using a sandwich ELISA following the protocol provided by BD Biosciences. A chemokine, MCP-1, in the serum from mice on Day 7, 10 and 14 after induction of EAE was also measured by using a sandwich ELISA following the protocol provided by BD Biosciences. All reagents, including recombinant mouse cytokines, chemokine and antibodies were purchased from BD Biosciences.

Analysis of infiltrating cells isolated from CNS

Mice were anaesthetized with diethyl ether on Day 14 after induction of EAE. After perfusion with PBS, brain and spinal cord were removed and homogenized. After washing with PBS, mononuclear cells were isolated using Ficoll gradient (Amersham Biosciences, Piscataway, NJ, USA) (Krakowski *et al.*, 1997). The cells were stained with APC-labelled anti-CD3 antibody, fluoroisothiocyanate (FITC) labelled anti-CD4 or CD8 or CD19 antibody (BD Biosciences) and were analysed by flow cytometer (BD FACS Calibur). Apoptosis of lymphocytes was analysed by using Annexin-5 apoptosis kit (BD Biosciences).

Pathological analysis

The brain and spinal cord were removed on Day 7, 10 and 14 after induction of EAE. Ten-micrometre frozen sections were fixed with acetone and stained with haematoxylin and eosin (HE), Luxol fast blue or antibodies of adhesion molecule ICAM-1 (CD54), vascular cell adhesion molecule-1 (VCAM-1: CD106), E-selectin (CD62E) and P-selectin (CD62P) (BD Biosciences), following the protocol provided by BD Biosciences.

Statistics

For statistic analysis, non-parametric Mann–Whitney *U*-test was used to calculate significant levels for all measurements. Values of $P < 0.05$ were considered statistically significant.

Results

Celecoxib inhibits EAE

To examine the effect of celecoxib on the development of EAE, we first administered celecoxib at the time of immunization with MOG_{35-55}. Oral administration of celecoxib reduced the incidence of disease and suppressed maximum EAE score and cumulative score compared with the control group (Fig. 1A, Table 1). Histological comparison between the thoracic region of the spinal cord demonstrated reduced monocyte infiltration and demyelination in cerecoxib-treated mice compared with vehicle-treated mice (Fig. 2A–D). Celecoxib was also effective in reducing the severity of disease when administered at Day 8

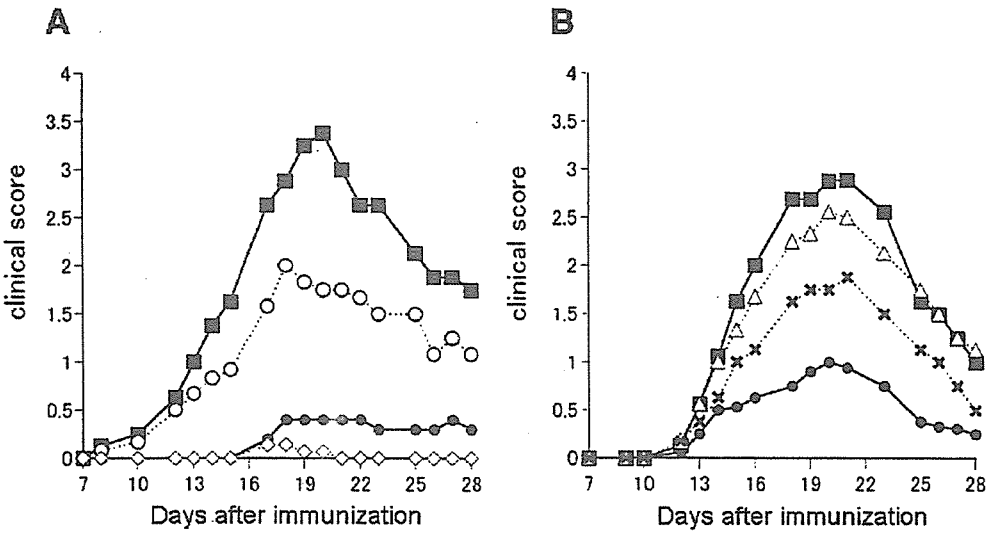

Fig. 1 Effect of celecoxib on actively induced EAE. EAE was induced in female B6 mice by immunization with MOG_{35-55} in CFA as described in Material and methods. (**A**) Mice were orally administered 5 μg/g (closed circles) or 10 μg/g (open diamond) of celecoxib starting from the day of the immunization, or with 5 μg/g of celecoxib starting from 8 days after the immunization (open circles). Control mice were administered vehicle alone (closed squares). Statistical analysis is shown in Table 1. (**B**) Mice were orally administered 5 μg/g of celecoxib (closed circles) or nimesulid (open triangle) or indomethacin (crosses) every 2 days from the day of EAE induction. Control mice were administered vehicle alone (closed squares). Statistical analysis is shown in Table 2. One representative experiment of two independent experiments is expressed as mean ± SEM.

Table 1 Clinical scores of EAE treated with celecoxib

	Max. score	Day of onset	Incidence (%)	Cumulative score
Control (CMC)	3.50 ± 0.20	12.50 ± 1.56	100 (10/10)	33.00 ± 5.05
Celecoxib 10 μg/g	0.14 ± 0.05*	17.50 ± 0.50	20.0 (2/10)	0.42 ± 0.04*
Celecoxib 5 μg/g	0.40 ± 0.40*	17.00 ± 0.00	20.0 (2/10)	3.80 ± 3.80*
Celecoxib 5 μg/g (from Day 8)	2.42 ± 0.57	14.20 ± 1.83	83.3 (10/12)	20.17 ± 5.22

Four groups of mice were immunized with MOG_{35-55} peptide for induction of EAE. The control CMC solution, 5 or 10 μg/g of celecoxib diluted in CMC, was orally injected via a cannula every 2 days starting from Day 0 or 8 after induction of EAE. Mean ± SEM of the following parameters are shown: maximum score of EAE (Max. score), the days of EAE onset, incidence of paralysed mice among sensitized mice (Incidence) and summation of the clinical scores from Day 0 to 30 (Cumulative score). *$P < 0.05$ versus control.

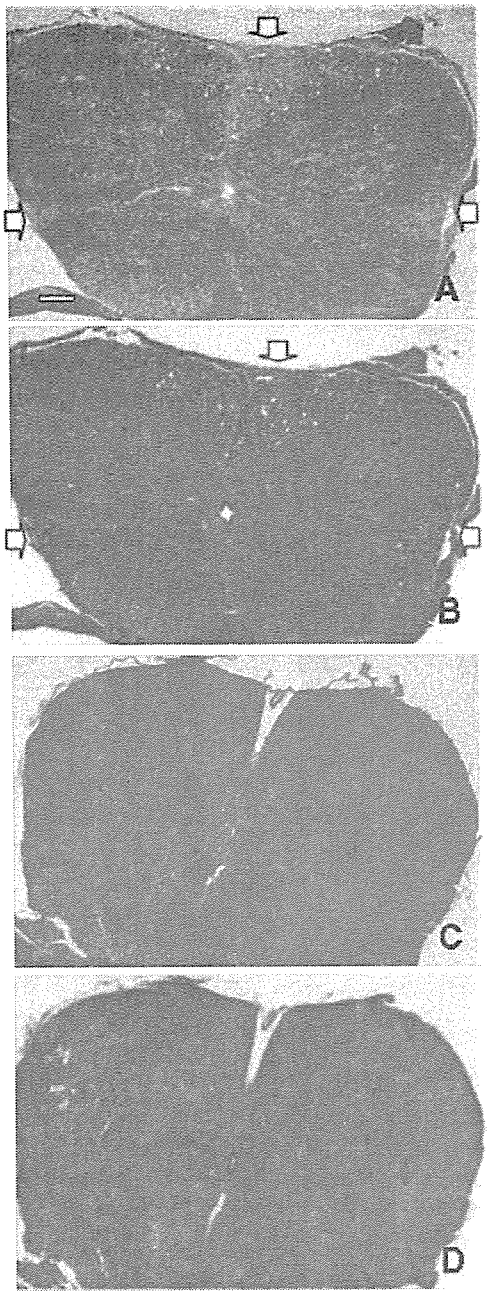

Fig. 2 Histopathological assessment of the CNS region in EAE-induced mice. Brains and spinal cords from EAE mice were removed on Day 14 after immunization as described in Material and methods. Thinly sliced (10 μm) frozen sections of the brains obtained from vehicle-treated mice (**A** and **B**) or celecoxib-treated mice (**C** and **D**) were stained with haematoxylin and eosin (**B** and **D**), or Luxol fast blue (**A** and **C**).

post-EAE-induction. Although indomethacin suppressed EAE to some extent, all mice died around Day 30 after immunization owing to intestinal ulcer. In contrast, oral administration of nimesulid, another COX-2 inhibitor, did not suppress either the incidence or the severity of EAE (Fig. 1B). Composite data from experiments is shown in Tables 1 and 2.

Celecoxib inhibits MOG-specific Th1 response

To determine the mechanisms by which celecoxib inhibits EAE, we examined the level of MOG-specific IgG1 and IgG2a in the serum samples collected from individual EAE-induced mice on Day 30. It is generally accepted that elevation of antigen-specific IgG2a antibody results from augmentation of a Th1 immune response to the antigen, whereas a higher level of IgG1 antibody would reflect a stronger Th2 response to the antigen. There was a significant elevation of the level of MOG_{35-55}-specific IgG1 and a slight reduction in the level of MOG-specific IgG2a in celecoxib-treated group compared with vehicle-treated group (Fig. 3A). In contrast, there was no significant difference in the level of either IgG1 or IgG2a in nimesulid-treated mice compared with vehicle-treated group (Fig. 3B).

To further investigate the response of T cells to MOG_{35-55} in celecoxib-treated mice, we examined the proliferative response and cytokine production of draining LN cells *in vitro*. Mice were immunized with MOG_{35-55} and were administered celecoxib or vehicle on the day of immunization. Ten days after immunization, draining LN cells were collected and cultured with MOG_{35-55} peptide. As shown in Fig. 4A, there was no significant difference in a proliferative response of MOG-reactive T cells between celecoxib-treated and vehicle-treated groups. We next examined the levels of cytokines in the culture supernatant by ELISA. The level of IFN-γ was reduced in the culture supernatants of LN cells obtained from mice treated with celecoxib compared with that from control mice (Fig. 4B). IL-4 and IL-10 were not detected in either culture supernatant. These results indicate that celecoxib reduces Th1 cytokine production from MOG-reactive T cells.

Celecoxib prevents EAE even in COX-2-deficient mice

Since another COX-2 inhibitor, nimesulid, did not have the inhibitory effect on EAE, we examined whether celecoxib could inhibit EAE in COX-2-deficient mice. As shown in Fig. 5A, the maximum EAE score, the day of onset and the severity of EAE were not significantly different between $COX\text{-}2^{-/-}$ and wild-type mice. Administration of celecoxib prevented the development of EAE in $COX\text{-}2^{-/-}$ mice as well as in wild-type mice. Consistent with the severity of EAE, the levels of MOG-specific IgG1 and IgG2a in $COX\text{-}2^{-/-}$ mice were not different compared with wild-type B6 mice (Fig. 5B). Moreover, celecoxib treatment increased the level of MOG-specific IgG1 even in $COX\text{-}2^{-/-}$ mice, resulting in the elevation of IgG1 : IgG2a ratio similar to that in wild-type mice (CMC = 0.29, celecoxib = 3.00) and $COX\text{-}2^{-/-}$ mice (CMC = 0.42, celecoxib = 2.52). These results indicate that the effect on the inhibition of EAE

Table 2 Clinical scores of EAE treated with celecoxib or other non-steroidal anti-inflammatory drugs

	Max. score	Day of onset	Incidence (%)	Cumulative score	Death (%)
Control (CMC)	3.05 ± 0.20	13.10 ± 1.16	100 (10/10)	26.47 ± 5.13	10 (1/10)
Celecoxib	1.02 ± 0.53*	14.30 ± 1.77	90 (9/10)	7.58 ± 6.72*	0 (0/10)
Nimesulid	2.54 ± 0.68	13.50 ± 1.56	100 (10/10)	22.15 ± 4.75	0 (0/10)
Indomethacin	1.70 ± 0.83	13.90 ± 1.93	100 (10/10)	15.21 ± 3.89	100 (10/10)*

Each mouse was immunized with MOG_{35-55} peptide for induction of EAE. The control CMC solution, or 5 μg/g of drugs diluted in CMC, was orally administered via a cannula every other day. Mean ± SEM of the following parameters are shown: maximum score of EAE (Max. score), the days of EAE onset, incidence of paralysed mice among sensitized rats (Incidence), summation of the clinical scores from Day 0 to 30 (Cumulative score) and the incidence of death during EAE (Death). *$P < 0.05$ versus control.

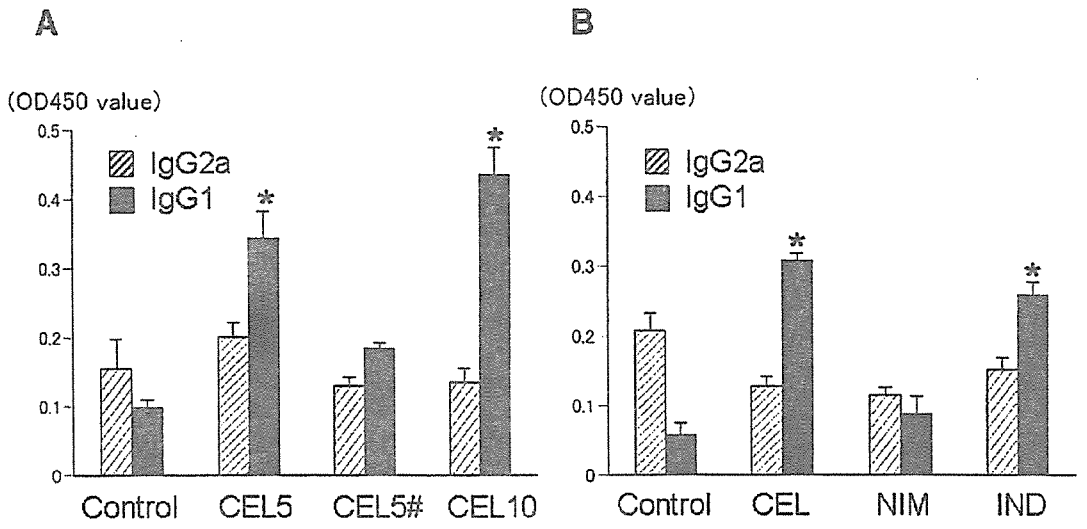

Fig. 3 Analysis of MOG_{35-55} IgG1 and IgG2a in EAE-induced mice. The relative titers of anti-MOG IgG1 and IgG2a in serum samples from individual mice ($n = 10$) on Day 30 after immunization were analysed as indicated in Methods. Data represent mean ± SEM. *$P < 0.05$ versus control. (a) Control = vehicle alone, CEL5 = 5 μg/g of celecoxib, CEL5# = 5 μg/g of celecoxib from Day 8 after the immunization, CEL10 = 10 μg/g of celecoxib. (b) Control = vehicle alone, CEL = celecoxib, NIM = nimesulid, IND = indomethacin.

and Th1 response by celecoxib is mediated by a COX-2-independent pathway (Table 3)

Celecoxib inhibits an infiltration of immune cells into CNS

To characterize the infiltrated cells into CNS, we isolated mononuclear cells from CNS obtained from celecoxib-treated or vehicle-treated mice. Mononuclear cells isolated from the CNS of vehicle-treated mice include $CD3^+$ T cells that comprised >80% of $CD4^+$ cells. In mice treated with celecoxib, the number of infiltrated cells was less than one-seventh compared with vehicle-treated mice (Table 4). In addition, we analysed apoptotic cells from CNS, spleen and draining LNs using annexin-5 staining. There was no difference in the frequency of apoptotic cells in all organs examined from celecoxib-treated and vehicle-treated mice (data not shown). These results suggest that celecoxib inhibits an infiltration of inflammatory cells into the CNS rather than induction of apoptosis of autoreactive T cells.

Celecoxib suppresses the expression of adhesion molecules and a chemokine related to cell infiltration into CNS

For the recruitment of autoreactive T cells into the brain through the blood–brain barrier (BBB), some adhesion molecules such as ICAM-1, VCAM-1 and P-selectin, and chemokines such as MCP-1 are required (Engelhardt *et al.*, 1997; Hofmann *et al.*, 2002). We performed an immunohistostaining of sliced brain sections from mice with EAE using antibodies against adhesion molecules. ICAM-1, VCAM-1 and P-selectin (Fig. 6A, C and E) were expressed on choroid plexus in the brain obtained from EAE-induced mice. In contrast, in brains obtained from celecoxib-treated mice, the expression level of P-selectin and ICAM-1 was lower compared with the control (Fig. 6B, D and F). In addition, we examined the level of MCP-1, which is an important chemokine involved in recruiting autoreactive T cells into the brain. As shown in Table 5, the level of MCP-1 in the serum obtained from

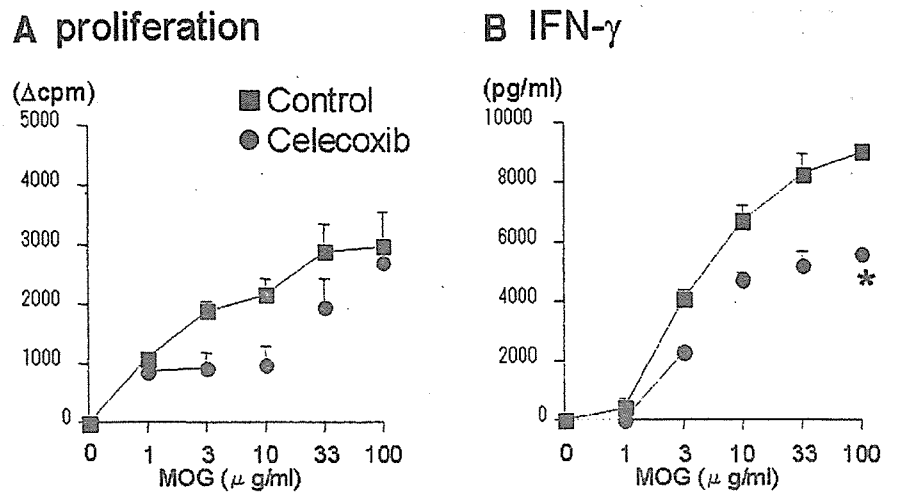

Fig. 4 Comparison of MOG_{35-55}-specific T-cell response after treatment with celecoxib. Popliteal and inguinal LN cells from treated and control animals were incubated in the presence of MOG_{35-55} for 48 h. Proliferative response was determined by the uptake of [^{3}H] thymidine (**A**), and IFN-γ was detected by ELISA (**B**). Representative data of two independent experiments are shown (n = 5 for each group). Error bars represent SEM. *P < 0.05 versus control.

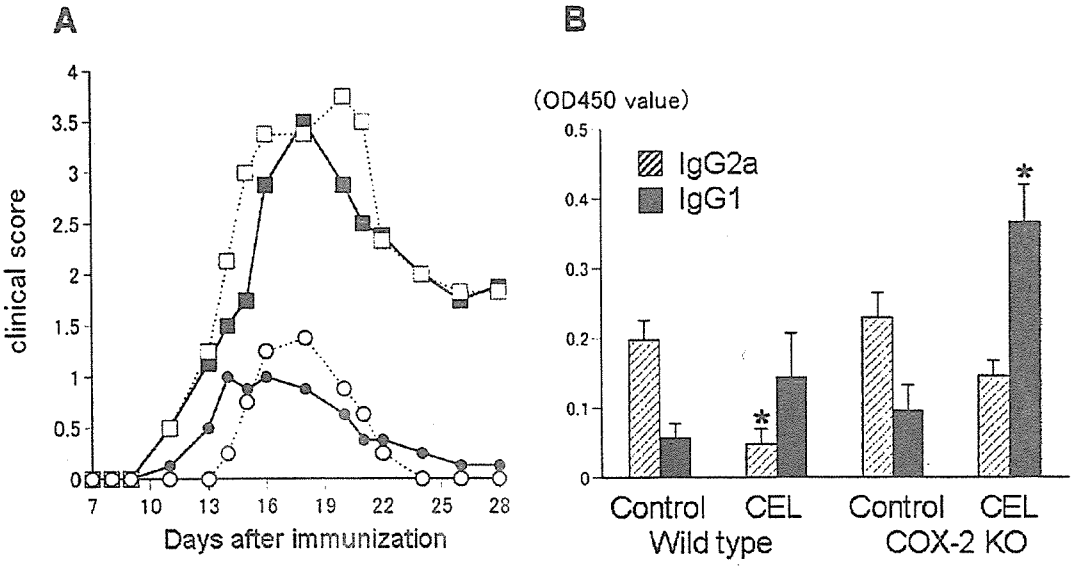

Fig. 5 Effect of celecoxib on actively induced EAE in COX-2-deficient mice. B6 mice and COX-2-deficient mice were immunized with MOG_{35-55} in CFA as described in Material and methods. (**A**) Mice were orally administered celecoxib (5 μg/g) every 2 days starting from the day of the immunization. Statistical analysis is shown in Table 3. Closed squares = vehicle alone for wild-type mice; closed circles = 5 μg/g of celecoxib for wild-type mice, open squares = vehicle alone for COX-2-deficient mice, open circles = 5 μg/g of celecoxib for COX-2-deficient mice. (**B**) The relative titres of anti-MOG IgG1 and IgG2a in serum samples from individual mice on Day 30 after immunization were analysed as indicated in Material and methods. Data represent mean ± SEM. *P < 0.05 versus control. Control = vehicle alone, CEL = celecoxib. One representative experiment of two independent experiments is expressed as mean ± SEM.

celecoxib-treated mice was significantly lower compared with that obtained from vehicle-treated mice. These findings suggested that celecoxib inhibits an infiltration of immune-mediated cells into CNS through the BBB by suppression of P-selectin, ICAM-1 and MCP-1.

Discussion

In the present study, we have demonstrated that a new-generation selective COX-2 inhibitor, celecoxib, strongly inhibited the development of EAE as compared with vehicle treatment or a traditional COX-2 inhibitor, nimesulid. The

Table 3 Clinical scores of EAE in COX-2-deficient mice

Mouse	Treatment	Max. score	Day of onset	Incidence (%)	Cumulative score
Wild-type	CMC	3.54 ± 0.28	12.60 ± 1.15	100 (10/10)	24.85 ± 6.37
	Celecoxib	1.13 ± 0.39*	13.20 ± 1.80	80 (8/10)	6.29 ± 4.02*
COX-2$^{-/-}$	CMC	3.75 ± 0.44	12.78 ± 1.57	100 (8/8)	29.88 ± 5.62
	Celecoxib	1.46 ± 0.51*	14.13 ± 1.96	87.5 (7/8)	5.39 ± 3.36*

Wild-type and COX-2$^{-/-}$ mice were immunized with MOG_{35-55} peptide to induce EAE. The control CMC solution, or 5 μg/g of celecoxib diluted in CMC, was administered every other day. Mean ± SEM of the following parameters are shown: maximum score of EAE (Max. score), the days of EAE onset, incidence of paralysed mice among sensitized mice (Incidence) and summation of the clinical scores from Day 0 to 30 (Cumulative score). *$P < 0.05$ versus control.

Table 4 Cell infiltration into the CNS of EAE-induced mice

	Mononuclear cell	$CD3^+$ cell	$CD4^+$ cell	$CD19^+$ cell
EAE mice				
Control (CMC)	667 ± 176	203 ± 69	158 ± 50	6 ± 1
Celecoxib	90 ± 57*	12 ± 8*	9 ± 5*	0 ± 0
Naive mice	20 ± 6	5 ± 2	3 ± 2	1 ± 0

CNS tissues from each group mouse were homogenized on Day 18 after immunization with MOG_{35-55} peptide. Mononuclear cells were isolated by Percoll solution. The cells were stained with cell markers and analysed by flow cytometer. Mean ± SEM of cell number (10^3 cells/mouse) is shown. Representative data of two independent experiments are shown ($n = 5$ for each group). *$P < 0.05$ versus control.

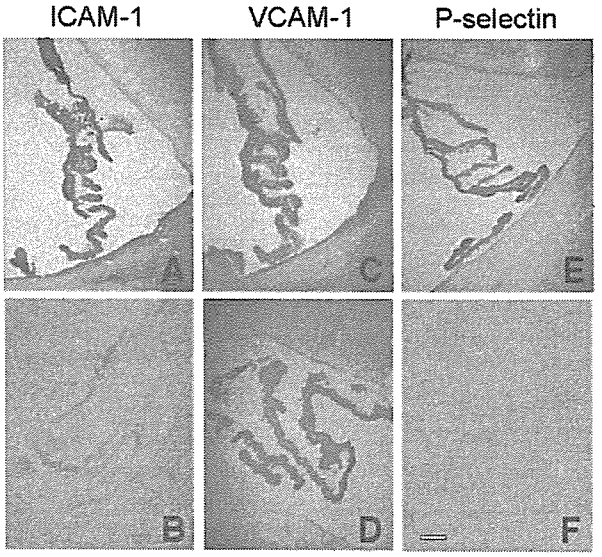

Fig. 6 Immunohistochemical staining with ICAM-1, VCAM-1 and P-selectin of the brain in EAE-induced mice. Brains from EAE mice were removed on Day 14 after immunization as described in Material and methods. Thinly sliced (10 μm) frozen sections of the brain were immunostained with anti-ICAM-1 antibody (**A** and **B**), anti-VCAM-1 antibody (**C** and **D**) and anti-P-selectin antibody (**E** and **F**). Figure shows choroid plexus region. Bar = 100 μm.

inhibitory effect on EAE by celecoxib was also evident in COX-2-deficient mice, indicating that celexoxib suppressed EAE in a COX-2-independent mechanism. In celecoxib-treated mice, MOG-specific Th1 responses were reduced and infiltration of immune cells was significantly inhibited compared with vehicle-treated mice, which were associated with lower expression of ICAM-1 and P-selectin on the choroid plexus in the brain.

Since EAE is an autoimmune inflammatory disease, administering COX-2 inhibitor was expected to inhibit disease as well as other COX inhibitors. Recently, Muthian *et al.* (2006) showed that some COX-2 inhibitors such as NS398 and LM01 suppressed EAE, when administered intraperitoneally every other day. In our study, we could not observe the inhibitory effect of nimesulid on EAE when orally administered every 2 days using the same conditions in which celecoxib exhibited a strong inhibitory effect. The route and timing of administration might be critical to modulate diseases. The inhibitory effect mediated by celecoxib was stronger compared with other COX inhibitors, suggesting that different mechanisms may be occurring in addition to the suppression of production of prostanoids that occurred at sites of disease and inflammation. In fact, COX-2 was not required for the celecoxib-mediated inhibitory effect on EAE. Recent studies have suggested that COX-2-independent pathways may contribute to celecoxib-mediated anti-tumour or anti-arthritic effect through enhanced apoptosis of tumour cells or synovial cells (Kusunoki *et al.*, 2002; Shishodia *et al.*, 2004). In our study, enhancing apoptosis of immune cells was not detected, indicating that different COX-2-independent mechanisms might be important for celecoxib-mediated inhibition of EAE. We observed that celecoxib treatment inhibited Th1 responses of MOG-reactive T cells. In the regulation of Th1/Th2 responses, prostaglandin E2 synthesized by COX has been reported to suppress IL-2 and IFN-γ production by a Th1 clone (Snijdewint *et al.*, 1993). In addition, Meyer *et al.* (2003) reported that administration of COX-2 inhibitor, NS398, increased *Helicobacter*-stimulated IL-12 and IFN-γ production, suggesting that COX-2 inhibition resulted in enhanced Th1 responses. In contrast, celecoxib inhibited Th1 responses of autoreactive T cells. Therefore, this COX-2-independent effect on immune system may be a mechanism to explain why celecoxib suppresses EAE to a greater degree compared with that of other COX-2 inhibitors. Allonza *et al.* (2006) reported that

Table 5 Serum level of MCP-1 in EAE mice after treatment with celecoxib

	Day 0	Day 7	Day 10	Day 14
EAE mice				
Control (CMC) (n = 18)	ND	60.0 ± 21.0	42.6 ± 17.0	ND
Celecoxib (n = 16)	ND	8.5 ± 5.0*	12.9 ± 8.5	ND
Naive mice (n = 10)	ND	ND	ND	ND

B6 mice were immunized with MOG_{35-55} peptide as described in Material and methods. Serum samples from individual mice were collected on Day 0, 7, 10 and 14 after immunization. Serum concentration of MCP-1 was measured by ELISA. Data represent mean ± SEM (pg/ml). ND = not detectable. *P < 0.05 versus control.

celecoxib inhibits IL-12 αβ and β2 folding and secretion in association with the increased interaction of IL-12 with calreticulin, an endoplasmic reticulum-resident chaperone in retention of misfolded cargo proteins, while blocking interaction with Erp44. They also demonstrated that an analogue of celecoxib lacking the COX-2 inhibitor activity showed identical effects to that of celecoxib on folding and secretion of IL-12, indicating that the effect is COX-2-independent. Since IL-12 is a key cytokine to provoke Th1 immune response, reduction in MOG-specific Th1 response is consistent with these previous findings.

The infiltration of immune cells in the CNS was significantly inhibited in celecoxib-treated mice. Celecoxib has been reported to reduce expression of P-selectin and ICAM-1 in experimental inflammatory models such as experimental colitis (Cuzzocrea *et al.*, 2001, 2002). In our study, we observed that celecoxib suppressed expression of P-selectin and ICAM-1 in the brain of EAE mice. Since P-selectin and ICAM-1 are the adhesion molecules involved in the recruitment of inflammatory cells into CNS (Engelhardt *et al.*, 1997; Dietrich, 2002; Scott *et al.*, 2004), inhibition of cellular infiltration by celecoxib might be mediated by the downregulation of the expression of adhesion molecules.

Chemokines are also required for recruitment of immune cells into the CNS. MCP-1 is reported to be an essential chemokine in EAE (Hofmann *et al.*, 2002). In the mouse model of atherosclerosis, Wang *et al.* (2005) reported that celecoxib decreased the inflammatory response and hyperplasia following vascular injury through inhibition of MCP-1 induction. We detected a decreased level of MCP-1 in the serum in celecoxib-treated mice on EAE. The suppression of MCP-1 by celecoxib might also contribute to the reduction of infiltrating cells into the CNS.

In conclusion, celecoxib has a potent therapeutic potential for EAE by inducing a Th2 bias and suppressing infiltration of inflammatory cells into the CNS through a COX-2-independent mechanism. Further analysis of celecoxib-mediated suppression of EAE will help drug development for multiple sclerosis. Celecoxib is hoped to be a new choice of the treatment of multiple sclerosis.

Acknowledgement

This study was supported by the Japan Research Foundation for Clinical Pharmacology.

References

Alloza I, Baxter A, Chen Q, Matthiesen R, Vanderbroeck K. Celecoxib inhibits interleukin-12 αβ and β2 folding and secretion by a novel COX2-independent mechanism involving chaperones of the endoplasmic reticulum. Mol Pharm 2006; 69: 1579–87.

Arico S, Pattingre S, Bauvy C, Gane P, Barbat A, Codogno P, et al. Celecoxib induces apoptosis by inhibiting 3-phosphoinositide-dependent protein kinase-1 activity in the human colon cancer HT-29 cell line. J Biol Chem 2002; 277: 27613–21.

Cuzzocrea S, Mazzon E, Serraino I, Dugo L, Centorrino T, Ciccolo A, et al. Celecoxib, a selective cyclo-oxygenase-2 inhibitor reduces the severity of experimental colitis induced by dinitrobenzene sulfonic acid in rats. Eur J Pharmacol 2001; 431: 91–102.

Cuzzocrea S, Mazzon E, Sautebin L, Dugo L, Serraino I, De Sarro A, et al. Protective effects of celecoxib on lung injury and red blood cells modification induced by carrageenan in the rat. Biochem Pharmacol 2002; 63: 785–95.

Deininger MH, Schluesener HJ. Cyclooxygenases-1 and -2 are differentially localized to microglia and endothelium in rat EAE and glioma. J Neuroimmunol 1999; 95: 202–8.

Dietrich JB. The adhesion molecule ICAM-1 and its regulation in relation with the blood-brain barrier. J Neuroimmunol 2002; 128: 58–68.

Engelhardt B, Vestweber D, Hallmann R, Schulz M. E- and P-selectin are not involved in the recruitment of inflammatory cells across the blood-brain barrier in experimental autoimmune encephalomyelitis. Blood 1997; 90: 4459–72.

Grosch S, Tegeder I, Niederberger E, Brautigam L, Geisslinger G. COX-2 independent induction of cell cycle arrest and apoptosis in colon cancer cells by the selective COX-2 inhibitor celecoxib. FASEB J 2001; 15: 2742–4.

Hofmann N, Lachnit N, Streppel M, Witter B, Neiss WF, Guntinas-Lichius O, et al. Increased expression of ICAM-1, VCAM-1, MCP-1, and MIP-1 alpha by spinal perivascular macrophages during experimental allergic encephalomyelitis in rats. BMC Immunol 2002; 6: 11.

Hsu AL, Ching TT, Wang DS, Song X, Rangnekar VM, Chen CS. The cyclooxygenase-2 inhibitor celecoxib induces apoptosis by blocking Akt activation in human prostate cancer cells independently of Bcl-2. J Biol Chem 2000; 275: 11397–403.

Krakowski ML, Owens T. The central nervous system environment controls effector CD4+ T cell cytokine profile in experimental allergic encephalomyelitis. Eur J Immunol 1997; 27: 2840–7.

Kumar V, Aziz F, Sercarz E, Miller A. Regulatory T cells specific for the same framework 3 region of the Vb8.2 chain are involved in the control of collagen II-induced arthritis and experimental autoimmune encephalomyelitis. J Exp Med 1997; 185: 1725–33.

Kusunoki N, Yamazaki R, Kawai S. Induction of apoptosis in rheumatoid synovial fibroblasts by celecoxib, but not by other selective cyclooxygenase 2 inhibitors. Arthritis Rheum 2002; 46: 3159–67.

Liu X, Yue P, Zhou Z, Khuri FR, Sun SY. Death receptor regulation and celecoxib-induced apoptosis in human lung cancer cells. J Natl Cancer Inst 2004; 96: 1769–80.

Meyer F, Ramanujam KS, Gobert AP, James SP, Wilson KT. Cutting edge: cyclooxygenase-2 activation suppresses Th1 polarization in response to Helicobacter pylori. J Immunol 2003; 171: 3913–7.

Miyamoto K, Oka N, Kawasaki T, Satoi H, Akiguchi I, Kimura J. The effect of cyclooxygenase-2 inhibitor on experimental allergic neuritis. Neuroreport 1998; 9: 2331–4.

Miyamoto K, Oka N, Kawasaki T, Satoi H, Matsuo A, Akiguchi I. The action mechanism of cyclooxygenase-2 inhibitor for treatment of experimental allergic neuritis. Muscle Nerve 1999; 22: 1704–9.

Miyamoto K, Oka N, Kawasaki T, Miyake S, Yamamura T, Akiguchi I. New cyclooxygenase-2 inhibitor for treatment of experimental autoimmune neuritis. Muscle Nerve 2002; 25: 280–2.

Muthian G, Raikwar HP, Johnson C, Rajasingh J, Kalgutkar A, Marnett LJ, et al. COX-2 inhibitors modulate IL-12 signaling through JAK-STAT pathway leading to Th1 response in experimental allergic encephalomyelitis. J Clin Immunol 2006; 26: 73–85.

Nakatsuji S, Terada N, Yoshimura T, Horie Y, Furukawa M. Effects of nimesulide, a preferential cyclooxygenase-2 inhibitor, on carrageenan-induced pleurisy and stress-induced gastric lesions in rats. Prostaglandins 1996; 55: 395–402.

Nicholson LB, Kuchroo VK. Manipulation of the Th1/Th2 balance in autoimmune disease. Curr Opin Immunol 1996; 8: 837–42.

Penning TD, Talley JJ, Bertenshaw SR, Carter JS, Collins PW, Docter S, et al. Synthesis and biological evaluation of the 1,5–diarylpyrazole class of cyclooxygenase-2 inhibitors: identification of 4-[5-(4-methylphenyl)-3-(trifluoromethyl)-1H-pyrazol-1-yl]benzene sulfonamide (SC-58635, celecoxib). J Med Chem 1997; 40: 1347–65.

Prosiegel M, Neu I, Mallinger J, Wildfeuer A, Mehlber L, Vogl S, et al. Suppression of experimental autoimmune encephalomyelitis by dual cyclooxygenase and 5-lipoxygenase inhibition. Acta Neurol Scand 1989; 79: 223–6.

Scott GS, Kean RB, Fabis MJ, Mikheeva T, Brimer CM, Phares TW, et al. ICAM-1 upregulation in the spinal cords of PLSJL mice with experimental allergic encephalomyelitis is dependent upon TNF-alpha production triggered by the loss of blood-brain barrier integrity. J Neuroimmunol 2004; 155: 32–42.

Shishodia S, Koul D, Aggarwal BB. Cyclooxygenase (COX)-2 inhibitor celecoxib abrogates TNF-induced NF-kappa B activation through inhibition of activation of I kappa B alpha kinase and Akt in human non-small cell lung carcinoma: correlation with suppression of COX-2 synthesis. J Immunol 2004; 173: 2011–22..

Simmons RD, Hugh AR, Willenborg DO, Cowden WB. Suppression of active but not passive autoimmune encephalomyelitis by dual cyclo-oxygenase and 5-lipoxygenase inhibition. Acta Neurol Scand 1992; 85: 197–9.

Snijdewint F, Kalinski P, Wierenga E, Bos J, Kapasenberg M. Prostaglandin E2 differentially modulate cytokine secretion profiles of human T helper lymphocytes. J Immunol 1993; 150: 5321.

Vane JR, Mitchell JA, Appleton I, Tomlinson A, Bishop-Bailey D, Croxtall J, et al. Inducible isoforms of cyclooxygenase and nitric oxide synthase in inflammation. Proc Natl Acad Sci USA 1994; 91: 2046–50.

Wang K, Tarakji K, Zhou Z, Zhang M, Forudi F, Zhou X, et al. Celecoxib, a selective cyclooxygenase-2 inhibitor, decreases monocyte chemoattractant protein-1 expression and neointimal hyperplasia in the rabbit atherosclerotic balloon injury model. J Cardiovasc Pharmacol 2005; 45: 61–7.

Warner TD, Mitchell JA. Cyclooxygenases: new forms, new inhibitors, and lessons from the clinic. FASEB J 2004; 18: 790–804.

Weber F, Meyermann R, Hempel K. Experimental allergic encephalomyelitis-prophylactic and therapeutic treatment with the cyclooxygenase inhibitor piroxicam (Feldene). Int Arch Allergy Appl Immunol 1991; 95: 136–41.

Xie WL, Chipman JG, Robertson DL, Erikson RL, Simmons DL. Expression of a mitogen-responsive gene encoding prostaglandin synthase is regulated by mRNA splicing. Proc Natl Acad Sci USA 1991; 88: 2692–6.

Zhang B, Yamamura T, Kondo T, Fujiwara M, Tabira T. Regulation of experimental autoimmune encephalomyelitis by natural killer (NK) cells. J Exp Med 1997; 186: 1677–87.

nature immunology

Invariant V_α19i T cells regulate autoimmune inflammation

J Ludovic Croxford[1], Sachiko Miyake[1], Yi-Ying Huang[2], Michio Shimamura[2] & Takashi Yamamura[1]

T cells expressing an invariant V_α19-J_α33 T cell receptor α-chain (V_α19i TCR) are restricted by the nonpolymorphic major histocompatibility complex class Ib molecule MR1. Whether V_α19i T cells are involved in autoimmunity is not understood. Here we demonstrate that T cells expressing the V_α19i TCR transgene inhibited the induction and progression of experimental autoimmune encephalomyelitis (EAE), a mouse model of multiple sclerosis. Similarly, EAE was exacerbated in MR1-deficient mice, which lack V_α19i T cells. EAE suppression was accompanied by reduced production of inflammatory mediators and increased secretion of interleukin 10. Interleukin 10 production occurred at least in part through interactions between B cells and V_α19i T cells mediated by the ICOS costimulatory molecule. These results suggest an immunoregulatory function for V_α19i T cells.

Two distinct mouse T cell subsets express invariant TCRα chains: V_α14-J_α18 (V_α14i; ref. 1) and V_α19-J_α33 (V_α19i; ref. 2). Although conventional T cells recognize peptide antigens presented by polymorphic major histocompatibility complex class Ia molecules, V_α14i 'invariant' T cell populations recognize nonpeptide antigens[3,4] presented in the context of the nonpolymorphic major histocompatibility complex class Ib molecule CD1d. MR1 may be able to present glycolipids *in vitro* to V_α19i T cells[5], but the identity or type of endogenous ligand recognized by V_α19i T cells *in vivo* is unknown. However, antigen recognition is essential for the development of T cells expressing V_α14i and V_α19i TCR chains, as these subsets are absent from *Cd1d1*$^{-/-}$ and *Mr1*$^{-/-}$ mice, respectively[6,7]. Similar invariant T cell subsets are present in humans[8,9]. Many of these cells also express natural killer (NK) cell markers on their surface (such as mouse NK1.1). Consequently, CD1d-restricted invariant T cells have traditionally been referred to as 'NKT cells' (V_α14i NKT cells)[10].

Transgenic overexpression of the V_α14i TCR chain protects against the development of mouse models of type 1 diabetes[11] and multiple sclerosis[12], suggesting that V_α14i NKT cells may be involved in regulating autoimmunity. In addition, susceptibility to type 1 diabetes is linked to quantitative and functional deficiencies in V_α14i NKT cells[13]. Mechanistic studies suggest that V_α14i NKT cells may down regulate autoimmunity by increasing the production of T helper type 2 (T_H2) cytokines[14–19]. However, in other conditions, NKT cells may promote the exacerbation of autoimmune disease. V_α14i NKT cell–deficient mice show ameliorated arthritis compared with that of their wild-type counterparts[18,20,21].

The immune function of MR1-restricted invariant T cells remains less clear than that of CD1d-restricted lymphocytes. MR1-restricted invariant T cells were first identified among human peripheral blood $CD4^-CD8^-$ T cells as a clonally expanded population expressing an invariant V_α7.2-J_α33 TCR chain (V_α7.2i T cells)[22]. Subsequent studies identified clonally expanded T cells expressing the highly homologous invariant V_α19-J_α33 TCR chain in mice and cattle[9]. V_α19i T cell development has been found to depend on the nonpolymorphic major histocompatibility complex class Ib molecule MR1 and on the presence of B cells[7]. The V_α19i TCR is uniquely overexpressed in the gut lamina propria and V_α19i T cell development depends on the presence of commensal gut flora, indicating potential involvement of these cells in gut immunity[2,7]. As MR1 molecules are thought to be retained in the endoplasmic reticulum, intestinal flora might provide exogenous ligands for the V_α19i TCR, or a cellular 'stress' signal, that enables transit of MR1 from the endoplasmic reticulum to the cell surface[2,7].

Human V_α7.2i T cells[2] but not mouse gut V_α19i T cells express NKT cell markers[7]. In contrast, the V_α19i TCR is expressed by most T cell hybridomas derived from liver $NK1.1^+$ T cells from *Cd1d1*$^{-/-}$ mice[23]. Furthermore, 25–50% of V_α19i cells from V_α19i transgenic mice on a *Tcra*$^{-/-}$ background express NK1.1 (ref. 24). Those divergent results regarding NK1.1 expression remain unclear, but may be due to differences among mouse genetic backgrounds. Alternatively, as with CD1d-restricted T cells, a subpopulation of MR1-restricted T cells may lack NK1.1 expression. Based on their predominant distribution in the gut, MR1-restricted T cells are often referred to as 'mucosal-associated invariant T cells'[2,7]. To avoid confusion, we subsequently use the term 'V_α19i T cells' to describe V_α19i T cells expressing NK1.1.

The V_α7.2i TCR is over-represented in central nervous system (CNS) lesions from multiple sclerosis autopsy samples[25], whereas the V_α24i TCR is mostly absent[26]. Those findings led us to speculate that MR1-restricted T cells may 'preferentially' migrate to CNS lesions,

[1]Department of Immunology, National Institute of Neuroscience, National Centre of Neurology and Psychiatry, Tokyo 187-8502, Japan. [2]Developmental Immunology Unit, Mitsubishi Kagaku Institute of Life Sciences, Tokyo 194-8511, Japan. Correspondence should be addressed to T.Y. (yamamura@ncnp.go.jp).

Received 26 May; accepted 5 July; published online 30 July 2006; doi:10.1038/ni1370

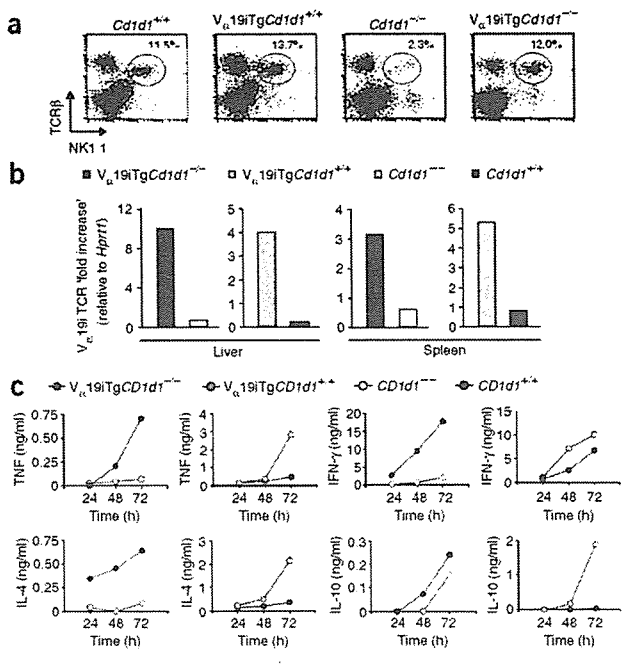

Figure 1 Characterization of NK1.1$^+$ T cells from V_α19iTg mice. (**a**) Flow cytometry of liver NK1.1$^+$ T cells 48 h after anti-asialo-GM1-mediated depletion of NK cells (mouse genotypes, above plots). Numbers above gated regions indicate the percentage of NK1.1$^+$TCRβ$^+$ cells. (**b**) Real-time RT-PCR of V_α19i TCR mRNA expression in liver or spleen NK1.1$^+$ T cells (mouse genotypes, key). Data are presented as 'fold increase' over expression of *Hprt1*. (**c**) Cytokines in the supernatants of sorted liver NK1.1$^+$ T cells (mouse genotypes, key) stimulated by immobilized anti-CD3 *in vitro*, measured at 24, 48 and 72 h after stimulation. Data are representative of two separate experiments (**a**,**b**) or the mean of two replicate values from two separate experiments (**c**).

where they regulate CNS inflammation. We designed this study to address the function of MR1-restricted T cells in experimental autoimmune encephalomyelitis (EAE)[14,17], a mouse model of multiple sclerosis. Here we report that over-representation of V_α19i T cells decreased the severity of EAE, whereas depletion of V_α19i T cells exacerbated EAE. Furthermore, V_α19i T cells exerted an influence on the phenotype and functions of autoimmune T cells in the draining lymph nodes and spleens of mice. In particular, over-representation of V_α19i T cells reduced the production of proinflammatory cytokines and increased the production of interleukin 10 (IL-10), which may account for V_α19i T cell–mediated suppression of autoimmune disease. Finally, interactions between V_α19i T cells and B cells mediated by the ICOS costimulatory molecule increased B cell IL-10 production and may therefore represent a mechanism by which V_α19i T cells regulate inflammation.

RESULTS

Characterization of transgenic V_α19i T cells

An antibody specific for the V_α19i TCR chain does not exist, and wild-type mice have very few MR1-restricted V_α19i T cells. Therefore, to circumvent those experimental hurdles and to evaluate the function of V_α19i T cells *in vivo*, we used V_α19i TCR–transgenic (V_α19iTg) mice[5], which were originally generated by injection into C57BL/6 mouse oocytes of a transgenic construct encoding a V_α19-J_α33 TCR construct driven by the endogenous *Tcra* promoter. We crossed the transgenic line with *Cd1d1*$^{+/+}$ and *Cd1d1*$^{-/-}$ C57BL/6 mice for seven to nine generations. First we compared numbers of liver NK1.1$^+$ T cells present in *Cd1d1*$^{+/+}$, *Cd1d1*$^{-/-}$, V_α19iTg*Cd1d1*$^{+/+}$ and V_α19iTg*Cd1d1*$^{-/-}$ mice (**Fig. 1a**). TCRβ$^+$NK1.1$^+$ T cells comprised 11.5% of total liver lymphocytes in *Cd1d1*$^{+/+}$ mice but only 2.3% of total liver lymphocytes in *Cd1d1*$^{-/-}$ mice. Therefore, most (about 80%) of NK1.1$^+$ T cells in *Cd1d1*$^{+/+}$ mice corresponded to CD1d-restricted V_α14i NKT cells, whereas about 20% were probably MR1 restricted[23]. Notably, V_α19iTg*Cd1d1*$^{-/-}$ mice had many NK1.1$^+$ T cells (12.0%), indicating that overexpression of the V_α19i TCR in *Cd1d1*$^{-/-}$ mice compensated for the reduction in NK1.1$^+$ T cells caused by CD1d deficiency. In contrast, the number of NK1.1$^+$ T cells was only slightly higher in V_α19iTg*Cd1d1*$^{+/+}$ mice, which had normal numbers of V_α14i NKT cells. To confirm that the NK1.1$^+$ T cell population in V_α19iTg mice was enriched in cells expressing the V_α19i TCR chain, we measured V_α19i mRNA transcripts in NK1.1$^+$ liver cells and splenocytes by real-time RT-PCR (**Fig. 1b**). V_α19i mRNA expression was much greater in liver and splenic NK1.1$^+$ T cell populations from V_α19iTg*Cd1d1*$^{+/+}$ or V_α19iTg*Cd1d1*$^{-/-}$ mice than in those from nontransgenic littermates (**Fig. 1b**). In V_α19i T cells, the V_α19i TCR chain 'preferentially' associates with TCRβ chains containing V_β8 or V_β6 segments[24]. Approximately 60–70% of liver NKT cells from V_α19iTg*Cd1d1*$^{-/-}$ or V_α19iTg*Tcra*$^{-/-}$ mice expressed either V_β8 or V_β6, compared with 30–40% of conventional T cells in the same mice (unpublished observations). These observations collectively demonstrate that NK1.1$^+$ T cell populations in V_α19iTg mice are highly enriched in cells expressing V_α19-J_α33 TCR chains and V_β6 or V_β8 TCR chains. Next we compared the ability of NK1.1$^+$ T cells from V_α19iTg and nontransgenic mice to produce immunosuppressive cytokines. To obtain V_α19i T cells, we depleted V_α19iTg*Cd1d1*$^{-/-}$ mice of NK cells by injecting antibody to

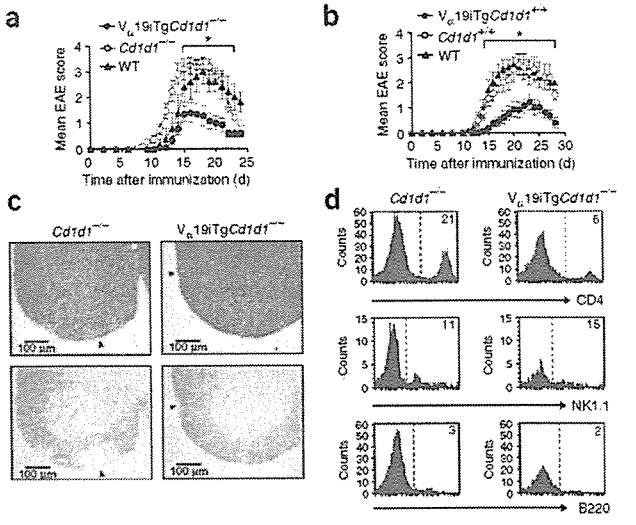

Figure 2 V_α19i T cells in EAE. (**a**,**b**) Clinical EAE scores of mice immunized with MOG(35–55). WT, wild-type. Data represent mean score ± s.e.m. from three independent experiments (n = 10–22 mice). (**c**) Monocyte infiltration and demyelination (arrowheads) of the lumbar spinal cord during EAE (day 15). (**d**) Quantification of spinal cord cellular infiltrates by flow cytometry. Areas to the right of dashed lines indicate positive cellular staining; numbers in histograms indicate percentage of CD4$^+$, NK1.1$^+$ (gated on CD3$^+$) or B220$^+$ cells. *, $P < 0.05$ (Mann-Whitney U-test). Data are representative of three separate experiments.

Table 1 V_α19i T cells in EAE

Group	Mice with EAE	Group score	EAE score	Day of onset
Wild-type	10 of 10	3.3 ± 0.3	3.3 ± 0.3	13.6 ± 0.7
Cd1d1$^{-/-}$	18 of 18	3.4 ± 0.2	3.4 ± 0.2	11.7 ± 0.5
V_α19iTg*Cd1d1*$^{-/-}$	13 of 22	1.3 ± 0.3***	2.2 ± 0.2**	14.3 ± 0.6**
Wild-type	7 of 7	3.6 ± 0.2	3.6 ± 0.2	13.6 ± 0.5
Cd1d1$^{+/+}$	11 of 11	3.3 ± 0.4	3.3 ± 0.4	14.8 ± 0.7
V_α19iTg*Cd1d1*$^{+/+}$	9 of 13	1.3 ± 0.3**	1.9 ± 0.4*	18.6 ± 1.2**
NK1.1$^-$ AdTx	10 of 10	3.6 ± 0.3	3.6 ± 0.3	11.6 ± 0.5
V_α19i AdTx	8 of 10	2.2 ± 0.4*	2.8 ± 0.3	15.8 ± 0.6***
Mr1$^{+/+}$	10 of 10	3.0 ± 0.2	3.0 ± 0.2	13.9 ± 0.5
Mr1$^{-/-}$	8 of 8	4.0 ± 0.0**	4.0 ± 0.0*	11.5 ± 0.5***

Clinical outcome of mice immunized with MOG(35–55) to induce EAE. Data represent number of mice with EAE (of total mice in group); mean group EAE score (± s.e.m.); mean EAE score excluding mice without evidence of EAE (± s.e.m.); and mean day of onset (± s.e.m.). In one experiment, mice received adoptive transfer (AdTx) of V_α19i T cells or NK1.1$^-$ cells as a control. *, $P < 0.05$, **, $P < 0.01$, and ***, $P < 0.001$, compared with control groups (Mann-Whitney U nonparametric test).

asialo-GM1 (anti-asialo-GM1). We then sorted NK1.1$^+$ cells from the liver. When activated by plate-bound anti-CD3, NK1.1$^+$ T cells from *Cd1d1*$^{+/+}$ mice secreted more interferon-γ (IFN-γ), tumor necrosis factor (TNF) and interleukin 4 (IL-4) than did those from *Cd1d1*$^{-/-}$ mice, confirming that CD1d-restricted T cells are a chief source of cytokines (**Fig. 1c**). However, NK1.1$^+$ T cells from V_α19iTg mice secreted more T_H1 cytokines (IFN-γ and TNF) and T_H2 cytokines (IL-4 and IL-10) than did NK1.1$^+$ T cells from nontransgenic littermates (**Fig. 1c**). During subsequent experiments, we used V_α19iTg*Cd1d1*$^{-/-}$ mice as a source of V_α19i T cells.

V_α19i T cells in EAE

To determine if an abundance of V_α19i T cells could modulate autoimmune disease, we analyzed the development and progression of EAE in V_α19iTg mice. We induced EAE by immunizing mice with a peptide of amino acids 35–55 of myelin oligodendrocyte glycoprotein (MOG(35–55)). The presence of the V_α19i transgene suppressed the development and progression of EAE, regardless of whether CD1d-restricted NKT cells were present (**Fig. 2a,b** and **Table 1**). The onset of EAE was delayed in V_α19iTg mice, and the incidence and severity of clinical EAE was reduced.

Histological examination of the lumbar (L3) region of the spinal cord 15 d after EAE induction showed less monocyte infiltration and demyelination (assessed by luxol fast blue staining) in V_α19iTg*Cd1d1*$^{-/-}$ mice than in *Cd1d1*$^{-/-}$ mice (**Fig. 2c**). In agreement with the histology, spinal cords of *Cd1d1*$^{-/-}$ mice contained three times more infiltrating cells than did those from V_α19iTg*Cd1d1*$^{-/-}$ mice (0.09×10^6 and 0.03×10^6 cells respectively, pooled from three mice). Flow cytometry showed fewer CD4$^+$ T cells infiltrating the CNS at an active stage of EAE (day 15) in V_α19iTg*Cd1d1*$^{-/-}$ mice (6%) than in nontransgenic littermates (21%; **Fig. 2d**). Moreover, 11% and 15% of CNS-infiltrating CD3$^+$ T cells expressed NK1.1$^+$ in *Cd1d1*$^{-/-}$ and V_α19iTg*Cd1d1*$^{-/-}$ mice, respectively, and NK1.1$^+$ T cells comprised between 1% and 2% of total CNS-infiltrating cells (**Fig. 2d**). Also, few B cells trafficked into the CNS during EAE (3% and 2% in *Cd1d1*$^{-/-}$ and V_α19iTg*Cd1d1*$^{-/-}$, respectively, **Fig. 2d**). To determine potential mechanisms of reduced CNS infiltration, we analyzed the expression of chemokine receptors and adhesion molecules necessary for T cell migration into the CNS. TCRβ$^+$CD4$^+$ T cells isolated from the CNS, lymph nodes and spleens of V_α19iTg*Cd1d1*$^{-/-}$ and *Cd1d1*$^{-/-}$ mice on day 18 after EAE induction had similar surface expression of CCR1 and CCR2 (data not shown). However, V_α19iTg*Cd1d1*$^{-/-}$ mice had fewer CD44$^+$ and CD49d$^+$ TCRβ$^+$ splenocytes than did *Cd1d1*$^{-/-}$ mice (**Supplementary Fig. 1** online).

Next we examined recall responses of MOG(35–55)-primed T cells by *ex vivo* rechallenge with MOG(35–55) on day 10 after disease induction. Compared with nontransgenic cells, lymph node cells from MOG(35–55)-primed V_α19iTg*Cd1d1*$^{-/-}$ mice produced less pro-inflammatory cytokines (IFN-γ, TNF, IL-2 and IL-17) and more immunosuppressive IL-10 ($P < 0.05$; **Fig. 3a**). IL-4 and IL-5 were below the limits of analysis detection (less than 5 pg/ml).

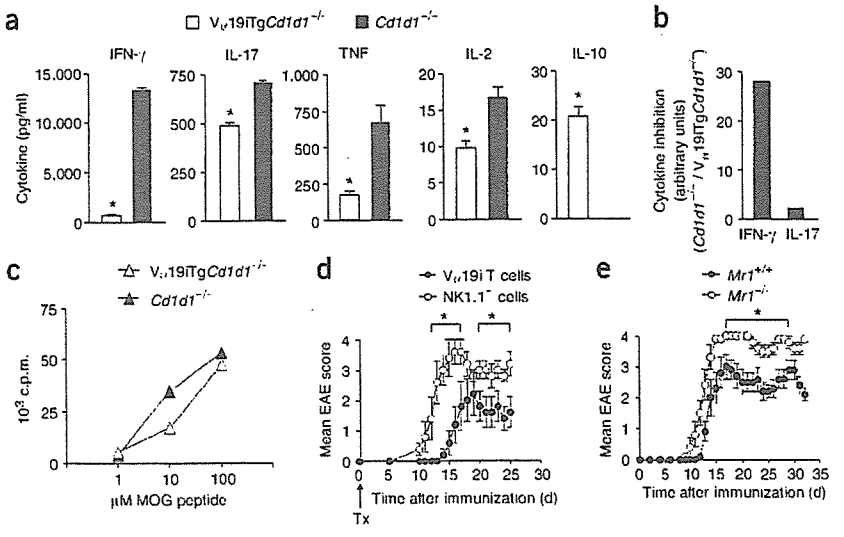

Figure 3 Inhibition of EAE is associated with decreased T_H1 cytokine production. (a) Cytometric bead assay of cytokines in the supernatants of MOG-specific lymph node cells (1×10^6) isolated from mice on day 10 after EAE induction and rechallenged with 100 μM MOG(35–55) *in vitro*, measured 72 h after rechallenge. Data represent the mean ± s.e.m. of duplicate samples from three separate experiments. *, $P < 0.05$ (two-tailed Student's *t*-test). (b) Inhibition of IFN-γ or IL-17 in V_α19iTg*Cd1d1*$^{-/-}$ mice versus *Cd1d1*$^{-/-}$ mice from a, presented as 'fold inhibition' of cytokine, calculated as the cytokine concentration from *Cd1d1*$^{-/-}$ mice divided by the cytokine concentration from V_α19iTg*Cd1d1*$^{-/-}$ mice. (c) T cell proliferation of cell preparations identical to those in a from lymph nodes (mouse genotypes, key) rechallenged for 72 h with varying doses of MOG(35–55), assessed by [^{3}H]thymidine incorporation. Data represent the mean of triplicate samples from three separate experiments. (d) Clinical EAE scores of wild-type nontransgenic mice ($n = 10$) that received 1×10^6 sorted V_α19i T cells or an equal number of NK1.1$^-$ TCRβ$^+$ liver cells from V_α19iTg*Cd1d1*$^{-/-}$ mice on the day of immunization with MOG(35–55). Tx indicates the day of adoptive transfer of cells. (e) Clinical EAE scores of *Mr1*$^{-/-}$ and *Mr1*$^{+/+}$ mice ($n = 8$–10) immunized with MOG(35–55). Data are representative of triplicate samples from three separate experiments.

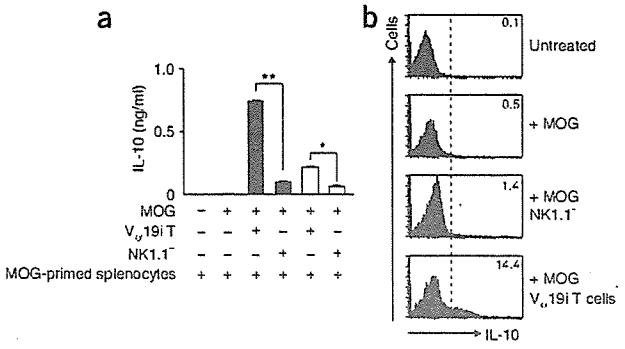

Figure 4 Interactions of V_α19i T cells and splenocytes induce IL-10. (a) Cytometric bead assay of IL-10 in the supernatants of liver V_α19i T cells from naive V_α19iTg*Cd1d1*$^{-/-}$ mice, cultured for 72 h with MOG(35–55)-specific splenocytes and MOG(35–55) (filled bars). In some cases, V_α19i T cells were separated from splenocytes by transwell inserts (open bars). Controls received NK1.1$^-$ liver cells from V_α19iTg*Cd1d1*$^{-/-}$ mice. Data represent ± s.e.m. from duplicate samples from three independent experiments. *, $P < 0.01$, and **, $P < 0.001$, compared with control (two-tailed Student's *t*-test). (b) Intracellular flow cytometry of IL-10 production by total cells from a. Areas to the right of dashed lines indicate positive cellular staining; numbers in histograms indicate percentages of IL-10-producing cells. Data are representative of three separate experiments.

IFN-γ secretion was more susceptible to the inhibitory effects of V_α19i T cells than was IL-17 (Fig. 3b). Splenocytes acted like lymph node cells (data not shown).

Overexpression of the V_α19i TCR might compromise the ability of conventional T cells to recognize myelin-derived peptides. However, the proliferative responses of MOG(35–55)-reactive T cells were not lower in V_α19iTg*Cd1d1*$^{-/-}$ mice, despite the inhibition of T_H1 cytokine production (Fig. 3c). Therefore, it is unlikely that the degree of EAE suppression seen in V_α19iTg*Cd1d1*$^{-/-}$ mice was the result of alterations in the MOG(35–55)-specific T cell repertoire. However, to exclude that possibility, we did adoptive transfer experiments. We transferred 1×10^6 V_α19i T cells isolated from V_α19iTg*Cd1d1*$^{-/-}$ mice into nontransgenic mice on the day of EAE induction. Mice that received TCRβ$^+$ T cells were significantly protected from EAE (Fig. 3d) and the onset of clinical disease was significantly delayed (Table 1) compared with that of mice that received V_α19i$^-$ NK1.1$^-$ T cells.

Next we sought to determine if V_α19i T cell deficiency could also influence clinical EAE. As no V_α19i-specific TCR antibody is available to deplete mice of V_α19i T cells *in vivo*, we used *Mr1*$^{-/-}$ mice, which lack V_α19i T cells[7]. As wild-type nontransgenic mice have about four times more V_α14i NKT cells than V_α19i T cells and *Cd1d1*$^{-/-}$mice did not show protection from EAE (Fig. 2a), we sought to determine whether the deletion of small numbers of MR1-restricted T cells could alter the clinical course of EAE. Compared with wild-type nontransgenic controls, *Mr1*$^{-/-}$ mice showed a significantly more severe form of EAE with an earlier onset ($P < 0.05$; Fig. 3e and Table 1). Furthermore, T cells from *Mr1*$^{-/-}$ mice proliferated more and produced more T_H1 cytokines and less IL-10 (data not shown). These experiments collectively suggest that V_α19i T cells have a regulatory function in a T_H1-mediated autoimmune disease.

V_α19i T cells induce B cell IL-10 production

MOG(35–55)-primed V_α19iTg lymph node cells and splenocytes secreted IL-10, which potently inhibits EAE[27–30] (Fig. 3a). Therefore, we sought to determine whether an increase in V_α19i T cells augmented general IL-10 production. To address that, we developed a mixed-lymphocyte assay in which we cultured NK1.1$^+$ or NK1.1$^-$ T cells from V_α19iTg*Cd1d1*$^{-/-}$ mice together with MOG(35–55)-primed nontransgenic splenocytes (Fig. 4a). Neither NK1.1$^+$ or NK1.1$^-$ T cells inhibited the proliferation of MOG(35–55)-primed splenic T cells restimulated with MOG(35–55) (data not shown). Cytokine analysis showed that the coculture supernatant contained considerable IL-10 (after stimulation with MOG(35–55)) in the presence of NK1.1$^+$ but not NK1.1$^-$ T cells from V_α19iTg*Cd1d1*$^{-/-}$ mice (Fig. 4a). NK1.1$^+$ T cells from V_α19iTg*Cd1d1*$^{-/-}$ mice induced IL-10 production even in the absence of MOG(35–55) ($P < 0.05$; Supplementary Fig. 2 online). However, IL-10 secretion was significantly enhanced in the presence of exogenous MOG(35–55) ($P < 0.01$; Supplementary Fig. 2). Intracellular cytokine analysis confirmed that IL-10 production was induced by the addition of NK1.1$^+$ but not NK1.1$^-$ T cells from V_α19iTg*Cd1d1*$^{-/-}$ mice (Fig. 4b). However, in the presence of transwell inserts, IL-10 production was inhibited, indicating that V_α19i T cell–mediated IL-10 production depends mainly on cell-cell contact (Fig. 4a). IL-4 and IL-5 were below the limit of detection (less than 5 pg/ml), and IFN-γ and TNF were slightly upregulated in the presence of V_α19i T cells (data not shown).

To determine which cells produced IL-10, in the same coculture experiment we analyzed IL-10 production by CD19$^+$, CD4$^+$, CD8$^+$,

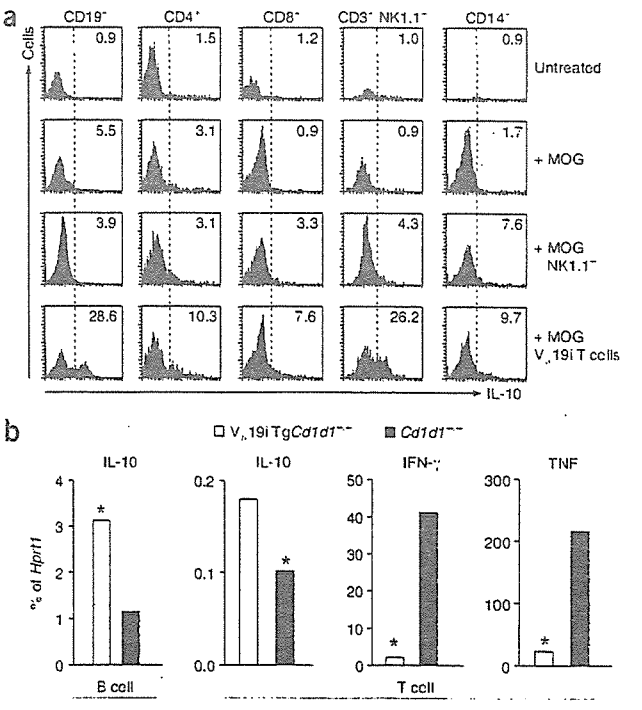

Figure 5 V_α19i T cells induce B cells to secrete IL-10. (a) Intracellular flow cytometry of IL-10 production by liver V_α19i T cells from naive V_α19iTg*Cd1d1*$^{-/-}$ mice, cultured for 72 h with MOG(35–55)-specific splenocytes and MOG(35–55). Areas to the right of dashed lines indicate positive cellular staining; numbers in histograms indicate percentage of IL-10-producing cells expressing various surface markers (above plots). Data are representative of two separate experiments. (b) Real-time RT-PCR of the expression of transcripts encoding various cytokines (above graphs) by splenic CD19$^+$ B cells or CD4$^+$ T cells sorted from mice with EAE. Data are expressed as a percentage of expression of *Hprt1* and are representative of two separate experiments. *, $P < 0.05$ (two-tailed Student's *t*-test).